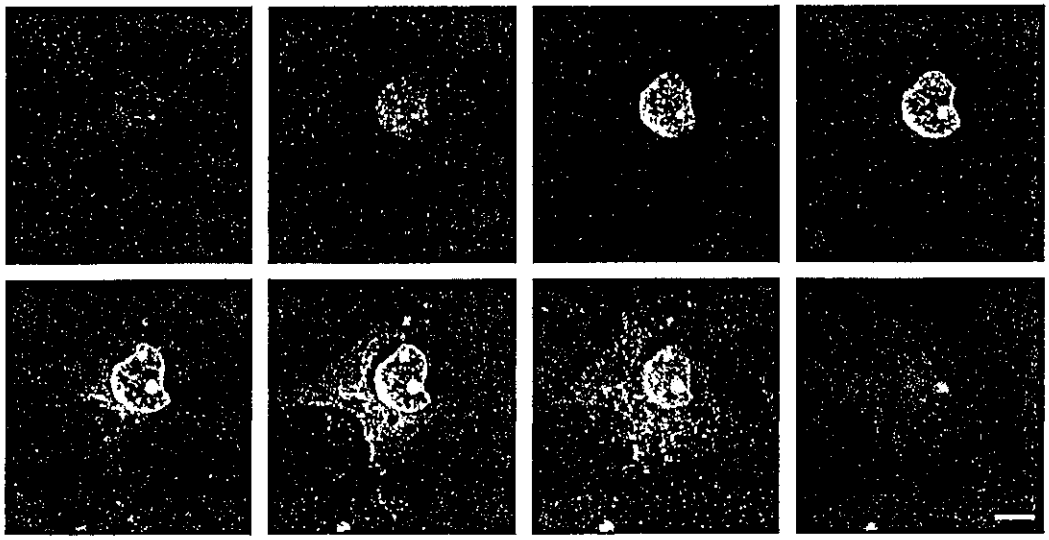

Fig. 4. R_{11}KC-conjugated QDs were accumulated in nucleous. Cells were stimulated by R_{11}KC-QD as described in Fig. 3. The cells were observed by confocal microscopy. The images are collected in the Z-direction at the span of 0.1 μm. Bars indicated 10 μm. Magnifications: ×120.

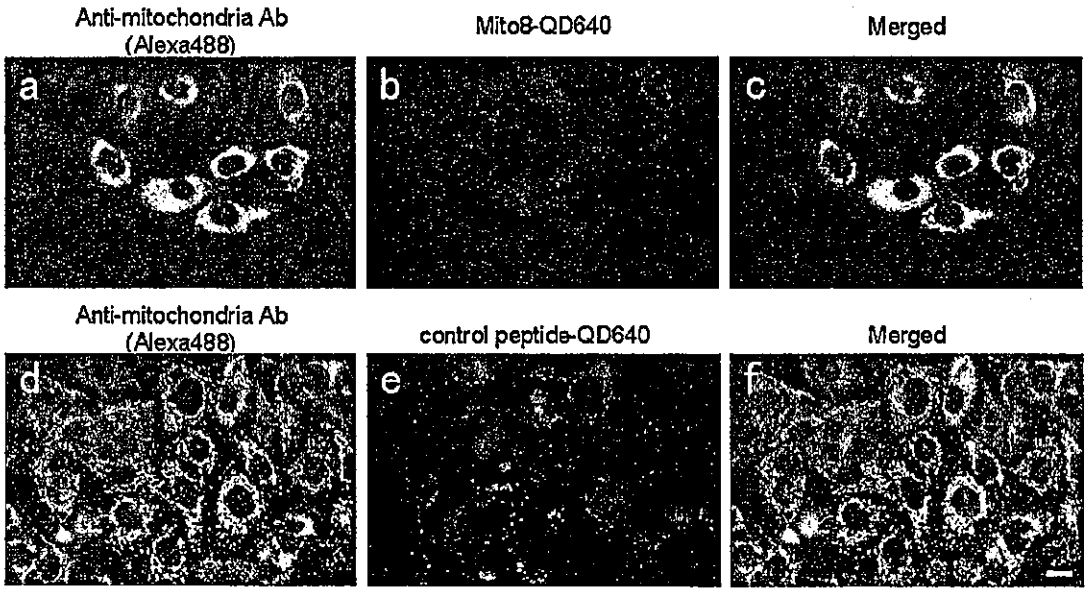

Fig. 5. Mitochondria images of Vero cells. Vero cells were stimulated with 1 μM with Mito-8 QD640 (a–c) or control START QD640 (d–f), and incubated for 12 hr under 37 C conditions. Cells were then fixed, and stained with anti-human mitochondria (M2) antibody. The cells were observed by fluorescent microscopy. Bars indicated 10 μm.

cence intensity enhanced remarkably after the secondary coupling with the target peptide (Fig. 2b). This result suggested that covering QD with the high molecular weight polymer such as polypeptides might prohibit the leakage of electron and might contribute to the continuative electron-rich condition of whole QD particle.

Next we evaluated whether the function of signal peptides would be held after conjugated with QDs. To confirm this, FITC-conjugated R_{11}KC peptides were conjugated with QD640 (fluorescence 640 nm, emitted red) and added to the cultured COS7 cells. We previously reported that QD without any peptides resulted in cellular-uptake into endosome by endocytotic pathways (17, 33). In this case, the red fluorescence from QD was located in nucleus and co-localized with that from FITC (Fig. 3a). This result indicated that QDs with nuclear peptides acquire another function that was based on R_{11}KC peptides. Unlabeled R_{11}KC remained in this study because the labeling efficiency of QDs with

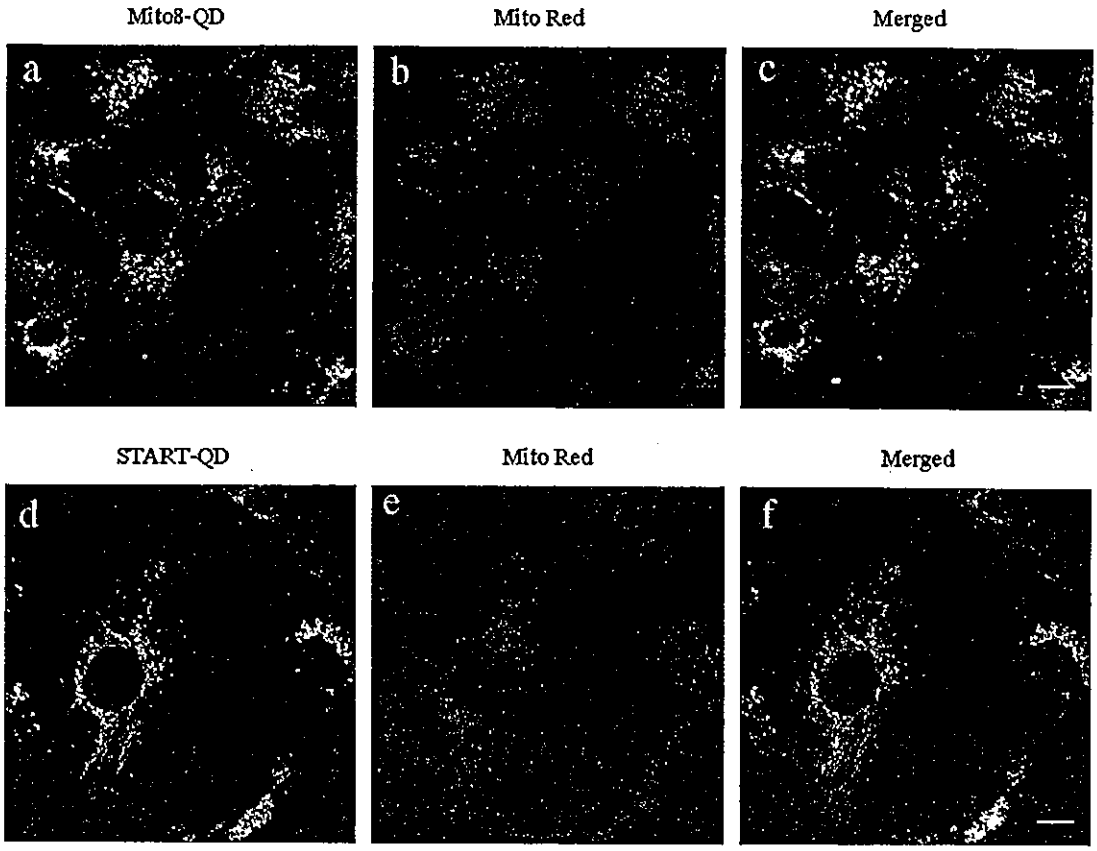

Fig. 6. Living mitochondria images by confocal microscope. Vero cells were cultured with 1 μM QD520-Mito8 (a–c) or QD520-START (control peptide, d–f) for 12 hr under 37 C conditions. Then cells were co-stimulated with MitoRed® mitochondria staining reagents (Dojindo Laboratories) for more additional 1 hr. After stimulation, cells were observed by confocal microscopy as shown in Fig. 4. Bars indicated 20 μm. Magnifications: ×80.

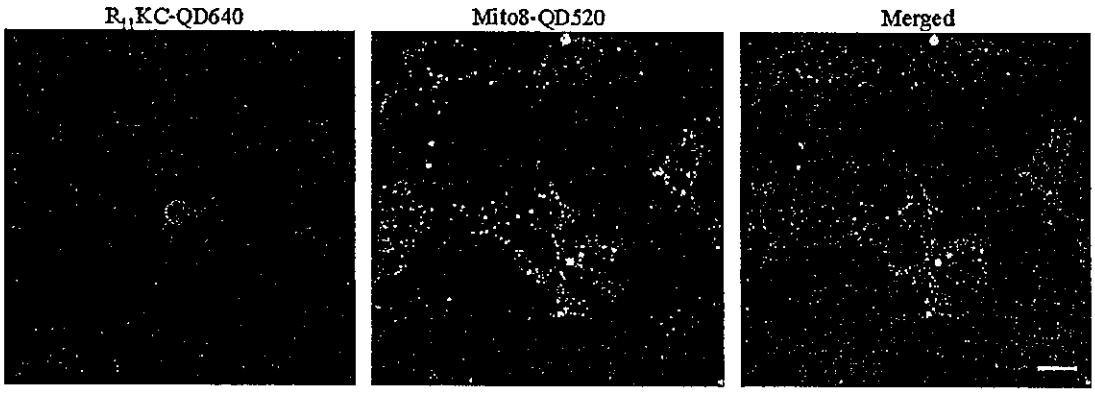

Fig. 7. Two kinds of signal peptide-QD showed independent behavior in the cells. Vero cells were co-stimulated with 1 μM QD640-Mito8 (emitted red) and QD-R_{11}KC (emitted green) for 12 hr under 37 C conditions. After fixed, the cells were observed by confocal microscopy. Bars indicated 20 μm.

oligopeptides was approximately 40% in this method and almost all of the FITC-tagged R_{11}KCs were not labeled with QDs. This result indicated that the R_{11}KC-QD has the same capability to localize into a nucleus as original ones. It is already reported that R_{11}KC peptide is rapidly localized into a nucleus by incubating for 10 min (25, 39). Then we tried to track the footmark of R_{11}KC peptide into nucleus in living cells for 15 min. Vero cells were treated with R_{11}KC-conjugated QD640 and continuously observed under a culture fluorescent microscopy (Fig. 3b). The penetration from the cell membrane to nuclei was observed about 30 sec after incubation, and precedently located into nucleus after 1 min. R_{11}KC-QDs were gradually accumulated the

whole nucleus during 15 min incubation. To investigate the localization of R_{11}KC-QDs into the nucleus, QDs distribution in the nucleus was observed by confocal microscopy (Fig. 4). R_{11}KC-QDs were dispersed in the whole nucleus and partially accumulated in nucleolus. In this study, we demonstrated that QDs as well as other fusion protein could also transit into nucleus with the help of nuclear signaling peptides.

Next we assessed the function of mitochondria signal peptides with QDs (Fig. 5). Mito-8 peptide- and control START peptide-coated QD640 (fluorescence 640 nm, emitted red) were incubated with cells and stained with anti-mitochondrial antibody. QD-red signal with Mito-8 gave raise to yellow in merged images (Fig. 5c). In contrast, red fluorescence emitted from control START peptides was not co-localized with that of mitochondria signal (Fig. 5f). Then we tried to visualize mitochondria distribution in living cells. Mito8-QD520 peptide was co-cultured with MitoRed® mitochondria staining dyes (Dojindo Laboratories, Japan). After incubation, the cells were observed by confocal laser microscopy (Fig. 6). QD-Mito-8 green luminescences from QD520 were also co-localized with conventional mitochondria probes. These results indicated that QDs with functional oligopeptides possessed dual functions to localize specific organelle and to emit high detectable fluorescence. Then we demonstrate the mixture of those two peptide separately move to their assigned organelle. The mixture of R_{11}KC-QD640 and Mito-8-QD520 were added to the Vero cells (Fig. 7). Red luminescence from R_{11}KC was separated from green ones from Mito-8 and not co-localized with each other, implying that QDs with functional peptides were individually transported to the target organelle.

Now several groups have reported that QDs conjugated with antibodies and some peptides for biological assays and cellular imaging *in vitro* and *in vivo* were demonstrated as brighter and longer lifetime probes (27–30). In this article, we demonstrated the various signal peptides conjugated with fluorescent QDs to both deliver QDs into living cells and selectively target specific organelles in living cells. In addition, these peptides-QD complexes have ability to translocate itself across the cell plasma membrane and can subsequently home to their specific targets such as the nucleus or the mitochondria. These results indicated that we succeeded in adding the new function as "information" to QDs by conjugating them with peptides. Our previous studies showed that QD-conjugated albumin and QD-glycerol can be targeted to the endosome and cytoplasm, respectively (14, 17). We showed in this article that QDs with targeted peptides can be also transported to nuclei and mitochondria. These techniques have the possibility that QDs can reveal transduction of proteins and peptides to specific subcellular compartments *in vitro* and even *in vivo* as a powerful tool for conducting intracellular analysis. We suggest that this technology could have a significant impact on the field of molecular and cellular biology as well as biotechnology. Recently, the plan that applied a novel nanomaterial such as nanocrystal QDs to the medical field attracted attention as one of the industrial applications of nanotechnology. And what is more, it is expected that QDs will be applied in the medical field for the innovative investigation, diagnosis and treatment of various diseases (8, 36, 38). It is very important to produce nanometer-sized materials with biological function, since we have no "designed material" which can arbitrarily penetrate nanometer-size gaps such as the skin, membrane, a blood vessel, and so on. This study demonstrates that these surface modifications of functional molecules combined with nanoparticles may work as bio-nanomachines conforming to the functions designated by their surface molecules. Nanomaterials have a great capacity of changing even the concept of existing diagnosis and medical treatment, by giving functions such as the pharmacological and magnetic effects, by giving the information of the specificity to tissue or organs *in vivo*. Novel nanomaterials including QD-supermolecules can be utilized as a transporter of the intracellular drug and gene delivery tools in the future.

We thank Mr. Kazuyuki Ito for valuable advice and help with proofreading. This work was supported by Medical Techniques Promotion Research Grant from the Ministry of Health, Labour and Welfare of Japan (H14-nano-004, Kenji Yamamoto).

References

1) Aglipay, J.A., Lee, S.W., Okada, S., Fujiuchi, N., Ohtsuka, T., Kwak, J.C., Wang, Y., Johnstone, R.W., Deng, C., Qin, J., and Ouchi, T. 2003. Oncogene **22**: 8931–8938.
2) Akerman, M.E., Chan, W.C., Laakkonen, P., Bhatia, S.N., and Ruoslahti, E. 2002. Nanocrystal targeting *in vivo*. Proc. Natl. Acad. Sci. U.S.A. **99**: 12617–12621.
3) Ballou, B., Lagerholm, B.C., Ernst, L.A., Bruchez, M.P., and Waggoner, A.S. 2004. Noninvasive imaging of quantum dots in mice. Bioconjugate Chem. **15**: 79–86.
4) Bruchez, M., Jr., Moronne, M., Gin, P., Weiss, S., and Alivisatos, A.P. 1998. Semiconductor nanocrystals as fluorescent biological labels. Science **281**: 2013–2016.
5) Chan, W.C., and Nie, S. 1998. Quantum dot bioconjugates for ultrasensitive nonisotopic detection. Science **281**: 2016–2018.
6) Dabboussi, B.O., Rodriguez-Viejo, J., Mikulec, F.V., Hein, J.R., Mattoussi, H., Ober, R., Jensen, K.F., and Bawendi, M.G. 1997. (CdSe)ZnS core-shell quantum dots; synthesis and characterization of size series of highly luminescent nanocrystallites. J. Phys. Chem. **101**: 9463–9475.

7) Dubertret, B., Skourides, P., Norris, D.J., Noireaux, V., Brivanlou, A.H., and Libchaber, A. 2002. *In vivo* imaging of quantum dots encapsulated in phospholipid micelles. Science **298**: 1759–1762.
8) Gao, X., Chan, W.C., and Nie, S. 2002. Quantum-dot nanocrystals for ultrasensitive biological labeling and multicolor optical encoding. J. Biomed. Opt. **7**: 532–537.
9) Gao, X., Cui, Y., Levenson, R.M., Chung, L.W.K., and Nie, S. 2004. *In vivo* cancer targeting and imaging with semiconductor quantum dots. Nat. Biotechnol. **22**: 969–976.
10) Gerion, D., Pinaud, F., Williams, S.C., Parak, W.J., Zanchet, D., Weiss, S., and Alivisatos, A.P. 2001. Synthesis and properties of biocompatible water-soluble silica-coated CdSe/ZnS semiconductor quantum dots. J. Phys. Chem. **105**: 8861–8871.
11) Goldman, E.R., Anderson, G.P., Tran, P.T., Mattoussi, H., Charles, P.T., and Mauro, J.M. 2002. Conjugation of luminescent quantum dots with antibodies using an engineered adaptor protein to provide new reagents for fluoroimmunoassays. Anal. Chem. **74**: 841–847.
12) Gorlich, D., and Mattaj, I.W. 1996. Nucleocytoplasmic transport. Science **271**: 1513–1518.
13) Haggie, P.M., and Verkman, A.S. 2002. Diffusion of tricarboxylic acid cycle enzymes in the mitochondrial matrix *in vivo*. Evidence for restricted mobility of a multienzyme complex. J. Biol. Chem. **277**: 40782–40788.
14) Hanaki, K., Momo, A., Oku, T., Komoto, A., Maenosono, S., Yamaguchi, Y., and Yamamoto, K. 2003. Semiconductor quantum dot/albumin complex is a long-life and highly photostable endosome marker. Biochem. Biophys. Res. Commun. **302**: 496–501.
15) Hines, M.A., and Guyot-Sionnest, P. 1996. Synthesis and characterization of strongly luminescing ZnS-capped CdSe nanocrystals. J. Phys. Chem. **100**: 468–471.
16) Hoshino, A., Fujioka, K., Oku, T., Suga, M., Sasaki, Y.F., Ohta, T., Yasuhara, M., Suzuki, K., and Yamamoto, K. 2004. Physicochemical properties and cellular toxicity of nanocrystal quantum dots depend on their surface modification. Nano Lett. **4**: 2163–2169.
17) Hoshino, A., Hanaki, K., Suzuki, K., and Yamamoto, K. 2004. The applications T-lymphoma labeled with fluorescent quantum dots to cell trafficking markers in a mouse body. Biochem. Biophys. Res. Commun. **314**: 46–53.
18) Ishii, D., Kinbara, K., Ishida, Y., Ishii, N., Okochi, M., Yohda, M., and Aida, T. 2003. Chaperonin-mediated stabilization and ATP-triggered release of semiconductor nanoparticles. Nature **423**: 628–632.
19) Jaiswal, J.K., Mattoussi, H., Mauro, J.M., and Simon, S.M. 2003. Long-term multiple color imaging of live cells using quantum dot bioconjugates. Nat. Biotechnol. **21**: 47–51.
20) Johnson, L.V., Walsh, M.L., and Chen, L.B. 1980. Localization of mitochondria in living cells with rhodamine 123. Proc. Natl. Acad. Sci. U.S.A. **77**: 990–994.
21) Kaether, C., and Gerdes, H.H. 1995. Visualization of protein transport along the secretory pathway using green fluorescent protein. FEBS Lett. **369**: 267–271.
22) Kaul, Z., Yaguchi, T., Kaul, S.C., Hirano, T., Wadhwa, R., and Taira, K. 2003. Mortalin imaging in normal and cancer cells with quantum dot immuno-conjugates. Cell Res. **13**: 503–507.
23) Larson, D.R., Zipfel, W.R., Williams, R.M., Clark, S.W., Bruchez, M.P., Wise, F.W., and Webb, W.W. 2003. Water-soluble quantum dots for multiphoton fluorescence imaging *in vivo*. Science **300**: 1434–1436.
24) Lidke, D.S., Nagy, P., Heintzmann, R., Arndt-Jovin, D.J., Post, J.N., Grecco, H.E., Jares-Erijman, E.A., and Jovin, T.M. 2004. Quantum dot ligands provide new insights into erbB/HER receptor-mediated signal transduction. Nat. Biotechnol. **22**: 198–203.
25) Matsushita, M., Tomizawa, K., Moriwaki, A., Li, S.T., Terada, H., and Matsui, H.J. 2001. A high-efficiency protein transduction system demonstrating the role of PKA in long-lasting long-term potentiation. J. Neurosci. **21**: 6000–6007.
26) Mattaj, I.W., and Englmeier, L. 1998. Nucleocytoplasmic transport: the soluble phase. Annu. Rev. Biochem. **67**: 265–306.
27) Mattoussi, H., Mauro, J.M., Goldman, E.R., Anderson, G.P., Sundar, V.C., Mikulec, F.V., and Bawendi, M.G. 2000. Self-assembly of CdSe-ZnS quantum dot bioconjugates using an engineered recombinant protein. J. Am. Chem. Soc. **122**: 12142–12150.
28) Medintz, I.L., Clapp, A.R., Mattoussi, H., Goldman, E.R., Fisher, B., and Mauro, J.M. 2003. Self-assembled nanoscale biosensors based on quantum dot FRET donors. Nat. Mater. **2**: 630–639.
29) Osaki, F., Kanamori, T., and Sando, S., Sera, T., and Aoyama, Y. 2004. Quantum dot conjugated sugar ball and its cellular uptake. On the size effects of endocytosis in the subviral region. J. Am. Chem. Soc. **126**: 6520–6521.
30) Pinaud, F., King, D., Moore, H.P., and Weiss, S. 2004. Bioactivation and cell targeting of semiconductor CdSe/ZnS nanocrystals with phytochelatin-related peptides. J. Am. Chem. Soc. **126**: 6115–6123.
31) Rizzuto, R., Brini, M., Pizzo, P., Murgia, M., and Pozzan, T. 1995. Chimeric green fluorescent protein as a tool for visualizing subcellular organelles in living cells. Curr. Biol. **5**: 635–642.
32) Rosenthal, S.J., Tomlinson, I., Adkins, E.M., Schroeter, S., Adams, S., Swafford, L., McBride, J., Wang, Y., DeFelice, L.J., and Blakely, R.D. 2002. Targeting cell surface receptors with ligand-conjugated nanocrystals. J. Am. Chem. Soc. **124**: 4586–4594.
33) Shibahara, A., Hoshino, A., Hanaki, K., Suzuki, K., and Yamamoto, K. 2004. On the cyto-toxicity caused by quantum dots. Microbiol. Immunol. **48**: 669–675.
34) Shubeita, G.T., Sekatskii, S.K., Dietler, G., Potapova, I., Mews, A., and Basch, T. 2003. Scanning near-field optical microscopy using semiconductor nanocrystals as a local fluorescence and fluorescence resonance energy transfer source. J. Microsc. **210**: 274–278.
35) Smith, A.M., Gao, X., and Nie, S. 2004. Quantum-dot nanocrystals for *in-vivo* molecular and cellular imaging. Photochem. Photobiol. (in press).
36) Su, X.L., and Li, Y. 2004. Quantum dot biolabeling coupled with immunomagnetic separation for detection of *Escherichia coli* O157:H7. Anal. Chem. **76**: 4806–4810.
37) Taguchi, T., Shimura, M., Osawa, Y., Suzuki, Y., Mizoguchi, I., Niino, K., Takaku, F., and Ishizaka, Y. 2004.

Nuclear trafficking of macromolecules by an oligopeptide derived from Vpr of human immunodeficiency virus type-1. Biochem. Biophys. Res. Commun. **320**: 18–26.

38) Voura, E.B., Jaiswal, J.K., Mattoussi, H., and Simon, S.M. 2004. Tracking metastatic tumor cell extravasation with quantum dot nanocrystals and fluorescence emission-scanning microscopy. Nat. Med. **10**: 993–998.

39) Wu, H.Y., Tomizawa, K., Matsushita, M., Lu, Y.F., Li, S.T., and Matsui, H. 2003. Poly-arginine-fused calpastatin peptide, a living cell membrane-permeable and specific inhibitor for calpain. Neurosci. Res. **47**: 131–135.

40) Wu, X., Liu, H., Liu, J., Haley, K.N., Treadway, J.A., Larson, J.P., Ge, N., Peale, F., and Bruchez, M.P. 2003. Immunofluorescent labeling of cancer marker Her2 and other cellular targets with semiconductor quantum dots. Nat. Biotechnol. **21**: 41–46.

41) Xu, H., Sha, M.Y., Wong, E.Y., Uphoff, J., Xu, Y., Treadway, J.A., Truong, A., O'Brien, E., Asquith, S., Stubbins, M., Spurr, N.K., Lai, E.H., and Mahoney, W. 2003. Multiplexed SNP genotyping using the Qbead system: a quantum dot-encoded microsphere-based assay. Nucleic Acids Res. **31**: 43.

American Journal of Pathology, Vol. 164, No. 1, January 2004

Role of Ubiquitin Carboxy Terminal Hydrolase-L1 in Neural Cell Apoptosis Induced by Ischemic Retinal Injury *in Vivo*

Takayuki Harada,*† Chikako Harada,*† Yu-Lai Wang,* Hitoshi Osaka,*‡ Kazuhito Amanai,† Kohichi Tanaka,†‡ Shuichi Takizawa,* Rieko Setsuie,*§ Mikako Sakurai,*§ Yae Sato,*§ Mami Noda,§ and Keiji Wada*

From the Department of Degenerative Neurological Diseases, National Institute of Neuroscience, National Center of Neurology and Psychiatry, Kodaira, Tokyo; Laboratory of Molecular Neuroscience,† School of Biomedical Science and Medical Research Institute, Tokyo Medical and Dental University, Tokyo; Precursory Research for Embryonic Science and Technology (PRESTO),‡ Japan Science and Technology Corporation (JST), Kawaguchi, Saitama; Laboratory of Pathophysiology,§ Graduate School of Pharmaceutical Sciences, Kyushu University, Higashi-ku, Fukuoka, Japan*

Ubiquitin is thought to be a stress protein that plays an important role in protecting cells under stress conditions; however, its precise role is unclear. Ubiquitin expression level is controlled by the balance of ubiquitinating and deubiquitinating enzymes. To investigate the function of deubiquitinating enzymes on ischemia-induced neural cell apoptosis *in vivo*, we analyzed gracile axonal dystrophy (*gad*) mice with an exon deletion for ubiquitin carboxy terminal hydrolase-L1 (UCH-L1), a neuron-specific deubiquitinating enzyme. In wild-type mouse retina, light stimuli and ischemic retinal injury induced strong ubiquitin expression in the inner retina, and its expression pattern was similar to that of UCH-L1. On the other hand, *gad* mice showed reduced ubiquitin induction after light stimuli and ischemia, whereas expression levels of antiapoptotic (Bcl-2 and XIAP) and prosurvival (brain-derived neurotrophic factor) proteins that are normally degraded by an ubiquitin-proteasome pathway were significantly higher. Consistently, ischemia-induced caspase activity and neural cell apoptosis were suppressed ~70% in *gad* mice. These results demonstrate that UCH-L1 is involved in ubiquitin expression after stress stimuli, but excessive ubiquitin induction following ischemic injury may rather lead to neural cell apoptosis *in vivo*. *(Am J Pathol 2004, 164:59–64)*

The small 76 amino acid protein ubiquitin plays a critical role in many cellular processes, including cell cycle control, transcriptional regulation, and synaptic development.[1,2] Although ubiquitin has been identified as a heat shock- and stress-regulated protein in several kinds of cells,[3,4] recent studies have shown that ubiquitin promotes either cell survival or apoptosis, depending on the stage of cell development or other cellular factors.[5–8] Ubiquitin expression level is controlled by the balance of ubiquitinating enzymes: ubiquitin-activating (E1), ubiquitin-conjugating (E2), ubiquitin-ligase (E3) enzymes, and deubiquitinating enzymes (DUBs). DUBs are subdivided into ubiquitin carboxy terminal hydrolases (UCHs) and ubiquitin-specific proteases (UBPs). Mammalian UCHs, UCH-L1, and UCH-L3 are both small proteins of ~220 amino acids that share >40% amino acid sequence identity.[9] However, the distribution of these isozymes is quite distinct in that UCH-L3 is distributed ubiquitously while UCH-L1 is selectively expressed in neuronal cells and in the testis/ovary.[9,10] UCH-L1 constitutes ~5% of the brain's total soluble protein, which demonstrates a possibility that it plays a major role in neuronal cell function.[11] Indeed, UCH-L1 is a constituent of cellular aggregates that are indicative of neurodegenerative disease, such as Lewy bodies in Parkinson's disease.[12] Furthermore, an isoleucine to methionine substitution at amino acid 93 of UCH-L1 is reported in a family with a dominant form of Parkinson's disease.[13] Recently, we found a UCH-L1 gene exon deletion in mice that causes gracile axonal dystrophy (*gad*), a recessive neurodegenerative disease.[14] These examples of neurodysfunction from UCH-L1 mutations in both humans and mice prompted us to investigate the function of UCH-L1 in ischemia-induced neuronal cell apoptosis. For this purpose, we evaluated the extent of ischemic injury in wild-type and *gad* mice retina. The retina was chosen as a model be-

Supported by grants from the Organization for Pharmaceutical Safety and Research, Japan Science and Technology Cooperation, the Ministry of Health, Labor and Welfare of Japan, and the Ministry of Education, Culture, Sports, Science and Technology of Japan.

C. H. was supported by the Japan Society for the Promotion of Science for Young Scientists.

Accepted for publication September 10, 2003.

Address reprint requests to Keiji Wada, M.D., Ph.D., Department of Degenerative Neurological Diseases, National Institute of Neuroscience, NCNP, 4-1-1 Ogawahigashi, Kodaira, Tokyo 187-8502, Japan. E-mail: wada@ncnp.go.jp.

cause it is a highly organized neural tissue. In addition, its layered construction is suitable for analysis of cell type-specific biological response against diverse stimuli.[15–18] Here, we show that the absence of UCH-L1 partially prevents ischemia-induced retinal cell apoptosis and propose its possible mechanisms.

Materials and Methods

Animals

We used homozygous *gad* mice[14] and their wild-type littermates between postnatal days 35 and 56. The *gad* mouse was found in the F2 offspring of CBA and RFM inbred strain mice and has been maintained by brother-sister mating for more than 10 years.[19] Mice were maintained and propagated at the National Institute of Neuroscience, National Center of Neurology and Psychiatry (Japan). Experiments using the mice were approved by the Animal Investigation Committee of the Institute. The animals were housed in a room with controlled temperature and fixed lighting schedule. Light intensity inside the cages ranged from 100 to 200 lux. For the analysis of light stress, the pupils were dilated with 0.5% phenylephrinezhydrochloride and 0.5% tropicamide, and the mice were exposed to 800~1300 lux of white fluorescent light for 30 minutes. Animals for negative controls were dark-adapted for 12 hours, and sacrificed under dim red light.

Immunohistochemistry

Animals were anesthetized with diethylether and perfused transcardially with saline, followed by 4% paraformaldehyde in 0.1 mol/L phosphate buffer containing 0.5% picric acid at room temperature. The eyes were removed and postfixed overnight in the same fixative at 4°C and embedded in paraffin wax. The posterior part of the eyes were sectioned saggitally at 7-μm thickness through the optic nerve, mounted and stained with hematoxylin and eosin. For immunohistochemical staining, the sections were incubated with phosphate-buffered saline (PBS) containing 10% normal donkey serum for 30 minutes at room temperature. They were then incubated overnight with a rabbit polyclonal antibody against ubiquitin (1:600; Chemicon, Temecula, CA) or mouse monoclonal antibody against UCH-L1 (1:200; Medac, Wedel, Germany). They were then visualized with fluorescein isothiocyanate (FITC)-conjugated goat anti-rabbit or anti-mouse IgG (Jackson Immunoresearch, West Grove, PA), respectively. The sections were examined by a confocal laser scanning microscope (Olympus, Tokyo, Japan).

Histology and Morphometric Studies

Ischemia was achieved and the animals were sacrificed as previously described.[16,17] Briefly, we instilled sterile saline into the anterior chamber of the left eye at 150 cm H_2O pressure for 15 minutes while the right eye served as a non-ischemic control. The animals were sacrificed 1 or 7 days after reperfusion, and eyes were enucleated for histological and morphometric studies. The posterior part of the eyes was sectioned sagittally at 7-μm thickness through the optic nerve, mounted and stained with hematoxylin and eosin. Ischemic damage after 7 days was quantified in two ways. First, the thickness of the inner retinal layer (IRL) [from the ganglion cell layer (GCL) to the inner nuclear layer (INL)] was measured with a calibrated reticle at ×80. Second, in the same sections, the number of cells in the GCL was counted from one ora serrata through the optic nerve to the other ora serrata. The changes of the number of ganglion cells after ischemia were expressed in ratio compared with the non-ischemic fellow eyes.

TUNEL Staining

Sections were incubated in 0.26 U/μl TdT in the supplied 1X buffer (Invitrogen, Carlsbad, CA), and 20 μmol/L biotinylated-16-dUTP (Roche, Basel, Switzerland) for 60 minutes at 37°C. Sections were washed three times in PBS (pH 7.4) and blocked for 30 minutes with 2% bovine serum albumin in PBS (pH 7.4). The sections were then incubated with FITC-coupled streptavidin (Jackson Immunoresearch), diluted 1:100 in PBS for 30 minutes, and examined with a confocal laser scanning microscope (Olympus).

Quantification of Retinal Cell Apoptosis and Caspase Activities

A mouse retina 1 day after ischemia was homogenized in 100 μl PBS containing 1 mmol/L phenylmethyl sulfonyl fluoride and centrifuged at 15,000 × *g* for 10 minutes. A portion of supernatant was used to quantify protein concentration, and the rest was processed for assays. Retinal cell apoptosis was quantified using the Cell Death ELISA kit (Roche). Caspase-1- and caspase-3-like activities were measured using caspase-1 and caspase-3 Colorimetric Assay Kits (Bio-vision, Mountain View, CA), respectively.

Western Blot Analysis

Western blots were performed as previously reported.[14] Five micrograms of total protein were loaded per lane. Primary antibodies used were Bcl-2 (1:500), Bcl-xL (1:500), XIAP (1:500) (all from Transduction Laboratories, Franklin Lakes, NJ), phosphorylated cyclic AMP responsive element-binding protein (PCREB) (1:500; Upstate Biotechnology, Waltham, MA) and brain-derived neurotrophic factor (BDNF) (1:500; Santa Cruz Biotechnology, Santa Cruz, CA). Blots were further incubated with an anti-mouse or rabbit IgG-horseradish peroxidase conjugate (1:10000; Chemicon). The Super Signal detection kit (Pierce, Rockford, IL) was used for visualization of immunoreactive bands.

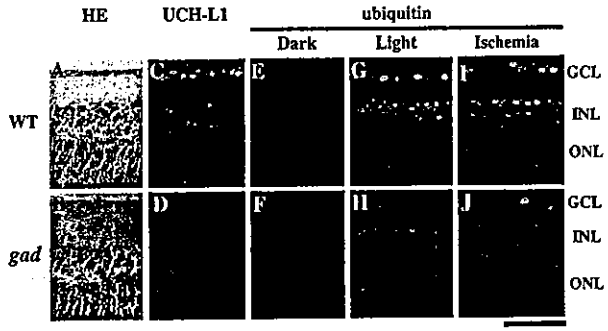

Figure 1. Functional loss of UCH-L1 decreases light- and ischemia-induced ubiquitin induction *in vivo*. Hematoxylin and eosin (HE) staining (**A** and **B**), immunostaining of UCH-L1 (**C** and **D**), immunostaining of ubiquitin in dark-reared (**E** and **F**), light-stressed (**G** and **H**) and ischemic (**I** and **J**) retina in wild-type (**A**, **C**, **E**, **G**, and **I**) and *gad* (**B**, **D**, **F**, **H**, and **J**) mice. Retinal structure is normal (**B**), but stress-induced ubiquitin induction is reduced (**H** and **J**) in *gad* mice. For the analysis of light stress (**G** and **H**), mice were exposed to 800 to 1300 lux of light for 30 minutes. Animals for negative controls were dark-adapted for 12 hours, and sacrificed under dim red light (**E** and **F**). Ischemic retina was prepared 1 day after ischemic injury (**I** and **J**). Bar, 50 μm.

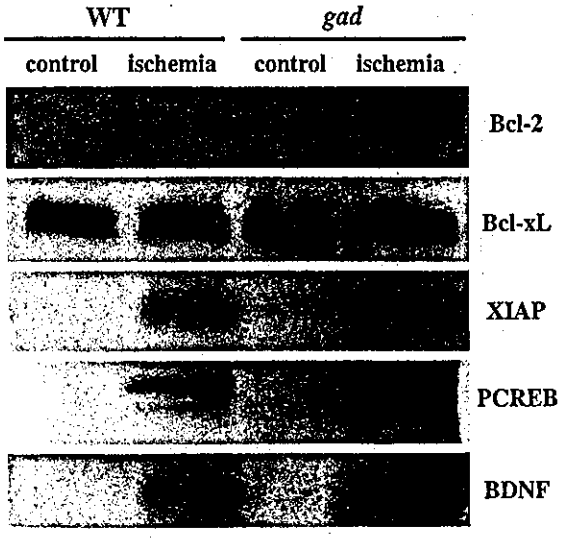

Figure 2. Immunoblot analysis of antiapoptotic and prosurvival proteins after ischemic injury. Five micrograms of total protein were prepared from whole retinas before (control) and 1 day after ischemic injury (ischemia). Representative image of four independent experiments are shown.

Results

Effect of UCH-L1 on Retinal Structure and Ubiquitin Expression

To determine the effect of UCH-L1 on retinal morphology, we examined the retinal tissue of *gad* mice with a UCH-L1 gene exon deletion.[14] Retinal structure in *gad* mice (Figure 1B) was normal compared with wild-type mice (Figure 1A). UCH-L1-like immunoreactivity was observed in the ganglion cell layer (GCL) and the inner nuclear layer (INL) in wild-type mice (Figure 1C) but was absent in *gad* mice (Figure 1D). Since ubiquitin is thought to be a stress protein,[1,20] we first examined the effect of the common oxidative stress for eye tissues, light stimuli, on ubiquitin induction.[20] Interestingly, ubiquitin was almost absent in both groups of animals, following dark adaptation (Figure 1, E and F). However, light stimuli strongly induced ubiquitin expression in the GCL and INL in wild-type mice (Figure 1G) but its induction level was very low in *gad* mice (Figure 1H). Ubiquitin expression pattern in wild-type mice was similar to that of UCH-L1 (Figure 1C). We next examined the effect of ischemia, severe oxidative stress,[21,22] on ubiquitin induction. As with light stimuli, ischemia induced strong ubiquitin expression in the GCL and INL (Figure 1I) and its induction was suppressed in *gad* mice (Figure 1J). These results demonstrate that retinal UCH-L1 plays an important role in ubiquitin induction[11] and *gad* mice retina is a useful model to investigate the effects of UCH-L1 on ischemic injury *in vivo*.

Effect of UCH-L1 on Antiapoptotic and Prosurvival Protein Expressions Following Ischemic Injury

The ubiquitin-proteasome pathway might be involved in non-neural cell apoptosis because this pathway can degradate antiapoptotic proteins such as Bcl-2 and XIAP *in vitro*.[5–8] To determine whether this is true for retinal cell apoptosis *in vivo*, we examined their protein expression levels in ischemic retinas (Figure 2). Ischemia-induced Bcl-2 protein level in *gad* mice was substantially higher than that of wild-type mice. Bcl-xL proteins (antiapoptotic member in the Bcl-2 family)[23,24] were examined at the same time as a control, but no obvious alternations were noted. On the other hand, XIAP protein[25,26] expression was apparently higher in *gad* mice. In addition to oxidative stress, ischemia induces calcium influx in neurons and triggers phosphorylation of cyclic AMP responsive element-binding protein (CREB).[27] PCREB can activate transcription of trophic factor proteins, such as BDNF, by binding to a critical calcium response element.[27] Since CREB is degraded by a ubiquitin-proteasome pathway by a phosphorylation-dependent mechanism,[28] we hypothesized a similar degradative pathway for CREB in ischemic retina. In wild-type mice, ischemia increased PCREB, but its expression level was much higher in *gad* mice. Consistent with PCREB up-regulation, BDNF protein expression was also higher in *gad* mice. Thus, excessive ubiquitin induction after ischemic injury may lead to the degradation of antiapoptotic proteins and suppression of the transcription of prosurvival proteins.[5–8,28]

Effect of UCH-L1 on Ischemia-Induced Neural Cell Apoptosis

To determine whether increased expression of antiapoptotic and prosurvival proteins in *gad* mice really leads to resistance against ischemia, we next examined the histology of ischemic retinas in both strains. As expected, ischemic damage in *gad* mice was mild compared with wild-type mice (Figure 3); the thickness of the inner retinal layer (IRL) (Figure 4A) and the percentage of surviving cells in the GCL (Figure 4B) after ischemia were significantly larger in *gad* mice. We also analyzed apoptotic cells in the retina by TUNEL staining. Control animals

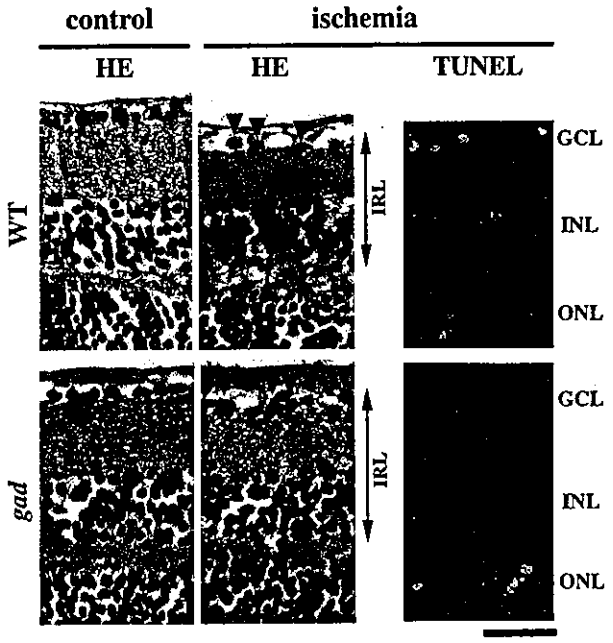

Figure 3. Representative pictures of HE staining (**left**) and TUNEL staining (**right**) in wild-type and *gad* mice retina before (control) and after ischemic injury (ischemia). Retinal damage 7 days after ischemia (HE staining) in *gad* mice was mild compared with wild-type mice. Consistently, TUNEL-positive cells 1 day after ischemia were observed only in the ONL in *gad* mice. Bar, 50 μm.

showed practically no signals in both strains (data not shown). However, in ischemic retinas, TUNEL-positive cells were observed in all three nuclear layers in wild-type mice, but mainly only in the outer nuclear layer (ONL) in *gad* mice (Figure 3). Consistently, quantitative analysis by ELISA demonstrated decreased retinal cell apoptosis in *gad* mice (Figure 4C). Ischemia-induced retinal cell apoptosis is executed by two distinct caspase proteases.

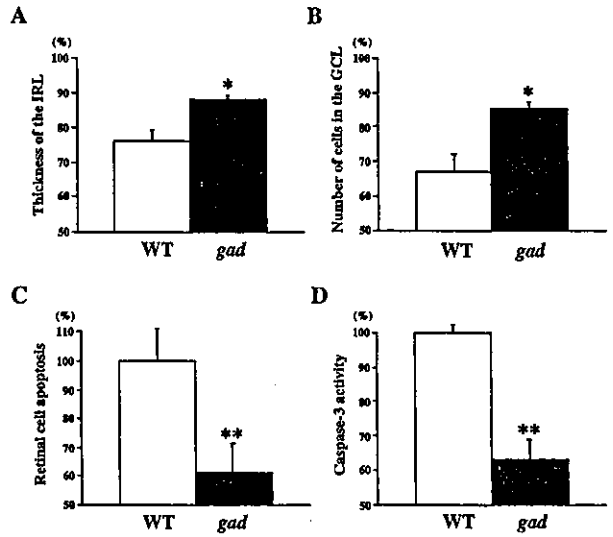

Figure 4. Effect of ischemic injury in wild-type and *gad* mice retina. Thickness of the IRL (arrows in Figure 3) (**A**) and the number of cells in the GCL (arrowheads in Figure 3) (**B**) in retina 7 days after ischemic injury as a percentage of the non-ischemic fellow eye. Quantitative analysis of retinal cell apoptosis (**C**) and caspase-3-like activity (**D**) in retina 1 day after ischemic injury. Results of six independent experiments are presented as mean ± SD (*, $P < 0.05$; **, $P < 0.01$).

Caspase-1 is predominantly associated with photoreceptor cell apoptosis in the ONL, whereas caspase-3 is more active in the GCL and INL for the same process.[29] To determine the mechanisms of strong tolerance against ischemia in *gad* mice, we next examined the activity of these two caspases in the ischemic retina. Caspase-1-like activity was not significantly different in *gad* mice compared with wild-type mice (80 ± 13%; P = not significant) (data not shown). On the other hand, caspase-3-like activity in *gad* mice was suppressed to 63 ± 6% compared with wild-type mice ($P < 0.01$) (Figure 4D).

Discussion

Ischemic injury is mainly associated with excessive concentrations of glutamate, which results in overactivation of glutamate receptors and initiates a cascade of events that leads to necrosis and/or apoptosis. Consistently, several studies have shown that retinal neurons can be protected by glutamate receptor antagonists.[17,30,31] An alternative strategy to attenuate glutamate neurotoxicity is keeping the extracellular glutamate concentration below neurotoxic levels. We previously demonstrated that selective inhibition of N-acetylated-α-linked-acidic dipeptidase (NAALADase), an enzyme responsible for the hydrolysis of neuropeptide N-acetyl-aspartyl-glutamate to N-acetyl-aspartate and glutamate, robustly protects neurons in a rat model of stroke[32] and in a mouse model of ischemic retinal injury.[17] Another possible target is the glutamate transporter.[33] There are four subtypes of glutamate transporters (GLAST, GLT-1, EAAC1, and EAAT5) in the retina.[16,33] By using GLAST and GLT-1 knockout mice,[34,35] we showed that both GLAST and GLT-1 (GLAST > GLT-1) are crucial for the protection of retinal cells from ischemic injury.[16]

In addition to these typical molecules involved in glutamate neurotoxicity, we first demonstrated that neuron-specific deubiquitinating enzyme, UCH-L1, is a new possible therapeutic target for ischemic retinal injury. In *gad* mice, functional loss of UCH-L1 results in the protection of retinal neurons following ischemic injury. One of the possible mechanisms is the accumulation of antiapoptotic proteins Bcl-2 and XIAP. Suppression of Bcl-2 leads to altered mitochondrial membrane permeability resulting in release of cytochrome c into the cytosol, which can trigger caspase activation leading to apoptosis.[23–26] On the other hand, a member of the IAP (inhibitor of apoptosis proteins) family, XIAP, can bind to and inhibit caspase-3 activation.[23–26] Consistently, retinal cell apoptosis in *gad* mice is suppressed mainly in the inner retina (Figure 3), where caspase-3 is more active than caspase-1.[27] These results suggest a possibility that functional loss of UCH-L1 may lead to decreased cytochrome c release from mitochondria and subsequent caspase inactivation in *gad* mice. If UCH-L1 inhibition works on the apoptotic pathway both before and after cytochrome c release from mitochondria,[23–26] this method may have a broader effect compared with the overexpression or suppression of a single antiapoptotic or apoptotic factor, respectively.

On the other hand, BDNF and PCREB protein expression levels were also up-regulated in *gad* mice. Recent studies have shown that trophic factors such as BDNF, ciliary neurotrophic factor (CNTF), basic fibroblast growth factor (bFGF), or glial cell line-derived neurotrophic factor (GDNF) increase RGC survival and regeneration.[36–45] Since CREB plays a central role in mediating responses of trophic factors including BDNF,[27] enhanced release of these trophic factors in *gad* mice may prevent ischemia-induced retinal cell apoptosis. We previously showed that, in addition to direct neuroprotection, these factors can alter secondary trophic factor production in retina-specific Müller glial cells, which indirectly regulate neural cell survival.[18,46] Consistently, intraocular injection of trophic factors induces the phosphorylated form of extracellular receptor kinase (pERK) or c-fos mainly in Müller cells.[47,48] Thus, loss of UCH-L1 may induce neural cell survival by stimulating both neural and glial cells.[18,46,49]

Ischemic retinal injury is implicated in a number of pathological states, such as retinal artery occlusion, glaucoma, and diabetic retinopathy.[16,17,30,31] Accordingly, the present results raise intriguing possibilities for the management of these pathological conditions by modifying the expression of UCH-L1 and activity of the ubiquitin-proteasome pathway.[50] Using this strategy with trophic factors,[18,46] NAALADase inhibitor,[17] glutamate transporter activators, such as bromocryptine,[51,52] or overexpression of GLAST or GLT-1,[16] may induce synergic effects on multiple cellular targets to prevent ischemia-induced neural cell apoptosis. However, due to the central function of the ubiquitin system in many basic cellular processes, modulation of this system can become a "double-edged sword".[1] Depletion of the free ubiquitin pool may cause accumulation of proteins that should be subjected to ubiquitin-dependent proteolysis. To address these critical issues, further investigations revealing the functional site of UCH-L1 and its involvement in ubiquitin induction *in vivo* will be needed.

Acknowledgments

We thank H.-M. A. Quah and L.F. Parada for critical reading of the manuscript, and members of the Wada lab for helpful discussions.

References

1. Hershko A, Ciechanover A, Varshavsky A: The ubiquitin system. Nat Med 2000, 6:1073–1081
2. DiAntonio A, Haghighi AP, Portman SL, Lee JD, Amaranto AM, Goodman CS: Ubiquitination-dependent mechanisms regulate synaptic growth and function. Nature 2001, 412:449–452
3. Finley D, Ozkaynak E, Varshavsky A: The yeast polyubiquitin gene is essential for resistance to high temperatures, starvation, and other stresses. Cell 1987, 48:1035–1046
4. Bond U, Agell N, Haas AL, Redman K, Schlesinger MJ: Ubiquitin in stressed chicken embryo fibroblasts. J Biol Chem 1988, 263:2384–2388
5. Dimmeler S, Breitschopf K, Haendeler J, Zeiher AM: Dephosphorylation targets Bcl-2 for ubiquitin-dependent degradation: a link between the apoptosome and the proteasome pathway. J Exp Med 1999, 189:1815–1822
6. Breitschopf K, Haendeler J, Malchow P, Zeiher AM, Dimmeler S: Posttranslational modification of Bcl-2 facilitates its proteasome-dependent degradation: molecular characterization of the involved signaling pathway. Mol Cell Biol 2000, 20:1886–1896
7. Daino H, Matsumura I, Takada K, Odajima J, Tanaka H, Ueda S, Shibayama H, Ikeda H, Hibi M, Machii T, Hirano T, Kanakura Y: Induction of apoptosis by extracellular ubiquitin in human hematopoietic cells: possible involvement of STAT3 degradation by proteasome pathway in interleukin 6-dependent hematopoietic cells. Blood 2000, 95:2577–2585
8. Yang Y, Fang S, Jensen JP, Weissman AM, Ashwell JD: Ubiquitin protein ligase activity of IAPs and their degradation in proteasomes in response to apoptotic stimuli. Science 2000, 288:874–877
9. Wilkinson KD, Lee KM, Deshpande S, Duerksen-Hughes P, Boss JM, Pohl J: The neuron-specific protein PGP 9.5 is a ubiquitin carboxyl-terminal hydrolase. Science 1989, 246:670–673
10. Wilkinson KD, Deshpande S, Larsen CN: Comparisons of neuronal (PGP 9.5) and non-neuronal ubiquitin C-terminal hydrolases. Biochem Soc Trans 1992, 20:631–637
11. Osaka H, Wang YL, Takada K, Takizawa S, Setsuie R, Li H, Sato Y, Nishikawa K, Sun YJ, Sakurai M, Harada T, Hara Y, Kimura I, Chiba S, Namikawa K, Kiyama H, Noda M, Aoki S, Wada K: Ubiquitin carboxy-terminal hydrolase L1 binds to and stabilizes monoubiquitin in neuron. Hum Mol Genet 2003, 12:1945–1958
12. Lowe J, McDermott H, Landon M, Mayer RJ, Wilkinson KD: Ubiquitin carboxyl-terminal hydrolase (PGP 9.5) is selectively present in ubiquitinated inclusion bodies characteristic of human neurodegenerative diseases. J Pathol 1990, 161:153–160
13. Leroy E, Boyer R, Auburger G, Leube B, Ulm G, Mezey E, Harta G, Brownstein MJ, Jonnalagada S, Chernova T, Dehejia A, Lavedan C, Gasser T, Steinbach PJ, Wilkinson KD, Polymeropoulos MH: The ubiquitin pathway in Parkinson's disease. Nature 1998, 395:451–452
14. Saigoh K, Wang YL, Suh JG, Yamanishi T, Sakai Y, Kiyosawa H, Harada T, Ichihara N, Wakana S, Kikuchi T, Wada K: Intragenic deletion in the gene encoding ubiquitin carboxy-terminal hydrolase in gad mice. Nat Genet 1999, 23:47–51
15. Harada T, Imaki J, Hagiwara M, Ohki K, Takamura M, Ohashi T, Matsuda H, Yoshida K: Phosphorylation of CREB in rat retinal cells after focal retinal injury. Exp Eye Res 1995, 61:769–772
16. Harada T, Harada C, Watanabe M, Inoue Y, Sakagawa T, Nakayama N, Sasaki S, Okuyama S, Watase K, Wada K, Tanaka K: Functions of the two glutamate transporters GLAST and GLT-1 in the retina. Proc Natl Acad Sci USA 1998, 95:4663–4666
17. Harada C, Harada T, Slusher BS, Yoshida K, Matsuda H, Wada K: N-acetylated-α-linked-acidic dipeptidase inhibitor has a neuroprotective effect on mouse retinal ganglion cells after pressure-induced ischemia. Neurosci Lett 2000, 292:134–136
18. Harada T, Harada C, Nakayama N, Okuyama S, Yoshida K, Kohsaka S, Matsuda H, Wada K: Modification of glial-neuronal cell interactions prevents photoreceptor apoptosis during light-induced retinal degeneration. Neuron 2000, 26:533–541
19. Yamazaki K, Wakasugi N, Tomita T, Kikuchi T, Mukoyama M, Ando K: Gracile axonal dystrophy (GAD), a new neurological mutant in the mouse. Proc Soc Exp Biol Med 1988, 187:209–215
20. Naash MI, Al-Ubaidi MR, Anderson RE: Light exposure induces ubiquitin conjugation and degradation activities in the rat retina. Invest Ophthalmol Vis Sci 1997, 38:2344–2354
21. Bonfoco E, Krainc D, Ankarcrona M, Nicotera P, Lipton SA: Apoptosis and necrosis: two distinct events induced, respectively, by mild and intense insults with N-methyl-D-aspartate or nitric oxide/superoxide in cortical cell cultures. Proc Natl Acad Sci USA 1995, 92:7162–7166
22. Szabo ME, Haines D, Garay E, Chiavaroli C, Farine JC, Hannaert P, Berta A, Garay RP: Antioxidant properties of calcium dobesilate in ischemic/reperfused diabetic rat retina. Eur J Pharmacol 2001, 428: 277–286
23. Tsujimoto Y, Shimizu S: Bcl-2 family: life-or-death switch. FEBS Lett 2000, 466:6–10
24. Ranger AM, Malynn BA, Korsmeyer SJ: Mouse models of cell death. Nat Genet 2001, 28:113–118
25. Deveraux QL, Reed JC: IAP family proteins: suppressors of apoptosis. Genes Dev 1999, 13:239–252
26. Green DR: Apoptotic pathways: paper wraps stone blunts scissors. Cell 2000, 102:1–4

27. Finkbeiner S: CREB couples neurotrophin signals to survival messages. Neuron 2000, 25:11–14
28. Taylor CT, Furuta GT, Synnestvedt K, Colgan SP: Phosphorylation-dependent targeting of cAMP response element binding protein to the ubiquitin/proteasome pathway in hypoxia. Proc Natl Acad Sci USA 2000, 97:12091–12096
29. Katai N, Yoshimura N: Apoptotic retinal neuronal death by ischemia-reperfusion is executed by two distinct caspase family proteases. Invest Ophthalmol Vis Sci 1999, 40:2697–2705
30. Lipton SA: Retinal ganglion cells, glaucoma and neuroprotection. Prog Brain Res 2001, 131:712–718
31. Osborne NN, Melena J, Chidlow G, Wood JP: A hypothesis to explain ganglion cell death caused by vascular insults at the optic nerve head: possible implication for the treatment of glaucoma. Br J Ophthalmol 2001, 85:1252–1259
32. Slusher BS, Vornov JJ, Thomas AG, Hurn PD, Harukuni I, Bhardwaj A, Traystman RJ, Robinson MB, Britton P, Lu XC, Tortella FC, Wozniak KM, Yudkoff M, Potter BM, Jackson PF: Selective inhibition of NAALADase, which converts NAAG to glutamate, reduces ischemic brain injury. Nat Med 1999, 5:1396–1402
33. Tanaka K: Functions of glutamate transporters in the brain. Neurosci Res 2000, 37:15–19
34. Tanaka K, Watase K, Manabe T, Yamada K, Watanabe M, Takahashi K, Iwama H, Nishikawa T, Ichihara N, Kikuchi T, Okuyama S, Kawashima N, Hori S, Takimoto M, Wada K: Epilepsy and exacerbation of brain injury in mice lacking the glutamate transporter GLT-1. Science 1997, 276:1699–1702
35. Watase K, Hashimoto K, Kano M, Yamada K, Watanabe M, Inoue Y, Okuyama S, Sakagawa T, Ogawa S, Kawashima N, Hori S, Takimoto M, Wada K, Tanaka K: Motor discoordination and increased susceptibility to cerebellar injury in GLAST mutant mice. Eur J Neurosci 1998, 10:976–988
36. Mey J, Thanos S: Intravitreal injections of neurotrophic factors support the survival of axotomized retinal ganglion cells in adult rats in vivo. Brain Res 1993, 602:304–317
37. Cohen A, Bray GM, Aguayo AJ: Neurotrophin-4/5 (NT-4/5) increases adult rat retinal ganglion cell survival and neurite outgrowth in vitro. J Neurobiol 1994, 25:953–959
38. Mansour-Robaey S, Clarke DB, Wang YC, Bray GM, Aguayo AJ: Effects of ocular injury and administration of brain-derived neurotrophic factor on survival and regrowth of axotomized retinal ganglion cells. Proc Natl Acad Sci USA 1994, 91:1632–1636
39. Unoki K, LaVail MM: Protection of the rat retina from ischemic injury by brain-derived neurotrophic factor, ciliary neurotrophic factor, and basic fibroblast growth factor. Invest Ophthalmol Vis Sci 1994, 35: 907–915
40. Hammes HP, Federoff HJ, Brownlee M: Nerve growth factor prevents both neuroretinal programmed cell death and capillary pathology in experimental diabetes. Mol Med 1995, 1:527–534
41. Bosco A, Linden R: BDNF and NT-4 differentially modulate neurite outgrowth in developing retinal ganglion cells. J Neurosci Res 1999, 57:759–769
42. Yan Q, Wang J, Matheson CR, Urich JL: Glial cell line-derived neurotrophic factor (GDNF) promotes the survival of axotomized retinal ganglion cells in adult rats: comparison to and combination with brain-derived neurotrophic factor (BDNF). J Neurobiol 1999, 38:382–390
43. Di Polo A, Aigner LJ, Dunn RJ, Bray GM, Aguayo AJ: Prolonged delivery of brain-derived neurotrophic factor by adenovirus-infected Müller cells temporarily rescues injured retinal ganglion cells. Proc Natl Acad Sci USA 1998, 95:3978–3983
44. Koeberle PD, Ball AK: Neurturin enhances the survival of axotomized retinal ganglion cells in vivo: combined effects with glial cell line-derived neurotrophic factor and brain-derived neurotrophic factor. Neuroscience 2002, 110:555–567
45. Peterson WM, Wang Q, Tzekova R, Wiegand SJ: Ciliary neurotrophic factor and stress stimuli activate the Jak-STAT pathway in retinal neurons and glia. J Neurosci 2000, 20:4081–4090
46. Harada T, Harada C, Kohsaka S, Wada E, Yoshida K, Ohno S, Mamada H, Tanaka K, Parada LF, Wada K: Microglia-Müller glia cell interactions control neurotrophic factor production during light-induced retinal degeneration. J Neurosci 2002, 22:9228–9236
47. Wahlin KJ, Campochiaro PA, Zack DJ, Adler R: Neurotrophic factors cause activation of intracellular signaling pathways in Müller cells and other cells of the inner retina, but not photoreceptors. Invest Ophthalmol Vis Sci 2000, 41:927–936
48. Wahlin KJ, Adler R, Zack DJ, Campochiaro PA: Neurotrophic signaling in normal and degenerating rodent retinas. Exp Eye Res 2001, 73:693–701
49. Bringmann A, Reichenbach A: Role of Müller cells in retinal degenerations. Front Biosci 2001, 6:E72–E92
50. Nishikawa K, Li H, Kawamura R, Osaka H, Wang YL, Hara Y, Hirokawa T, Manago Y, Amano T, Noda M, Aoki S, Wada K: Alterations of structure and hydrolase activity of parkinsonism-associated human ubiquitin carboxyl-terminal hydrolase L1 variants. Biochem Biophys Res Commun 2003, 304:176–183
51. Yamashita H, Kawakami H, Zhang YX, Tanaka K, Nakamura S: Neuroprotective mechanism of bromocriptine. Lancet 1995, 346:1305
52. Yamashita H, Kawakami H, Zhang YX, Tanaka K, Nakamura S: Effect of amino acid ergot alkaloids on glutamate transport via human glutamate transporter hGluT-1. J Neurol Sci 1998, 155:31–36

Journal of Neurochemistry, 2004, 88, 1540–1546 doi:10.1046/j.1471-4159.2003.02288.x

Proteomic analysis of brain proteins in the gracile axonal dystrophy (*gad*) mouse, a syndrome that emanates from dysfunctional ubiquitin carboxyl-terminal hydrolase L-1, reveals oxidation of key proteins

Alessandra Castegna,* Visith Thongboonkerd,** Jon Klein,** Bert C. Lynn,*,†,‡ Yu-Lai Wang,§ Hitoshi Osaka,§,¶ Keiji Wada,§ and D. Allan Butterfield*,‡

*Department of Chemistry and Center of Membrane Sciences, †Core Proteomics Laboratory and ‡Sanders-Brown Center on Aging, University of Kentucky, Lexington, Kentucky 40506 USA

§Department of Degenerative Neurological Diseases, National Institute of Neuroscience, Tokyo, Japan

¶PRESTO, Japan Science and Technology Corporation, Saitama, Japan

**Kidney Disease Program and Proteomics Core Laboratory, University of Louisville, Louisville, Kentucky, USA

Abstract

Ubiquitin carboxyl-terminal hydrolase L-1 (UCH L-1) is a crucial enzyme for proteasomal protein degradation that generates free monomeric ubiquitin. Our previous proteomic study identified UCH L-1 as one specific target of protein oxidation in Alzheimer's disease (AD) brain, establishing a link between the effect of oxidative stress on protein and the proteasomal dysfunction in AD. However, it is unclear how protein oxidation affects function, owing to the different responses of proteins to oxidation. Analysis of systems in which the oxidized protein displays lowered or null activity might be an excellent model for investigating the effect of the protein of interest in cellular metabolism and evaluating how the cell responds to the stress caused by oxidation of a specific protein. The gracile axonal dystrophy (*gad*) mouse is an autosomal recessive spontaneous mutant with a deletion on chromosome 5 within the gene encoding UCH L-1. The mouse displays axonal degeneration of the gracile tract. The aim of this proteomic study on *gad* mouse brain, with dysfunctional UCH L-1, was to determine differences in brain protein oxidation levels between control and *gad* samples. The results showed increased protein oxidation in thioredoxin peroxidase (peroxiredoxin), phosphoglycerate mutase, Rab GDP dissociation inhibitor α/ATP synthase and neurofilament-L in the *gad* mouse brain. These findings are discussed with reference to the effect of specific protein oxidation on potential mechanisms of neurodegeneration that pertain to the *gad* mouse.

Keywords: Alzheimer's disease, amyotrophic lateral sclerosis, brain protein oxidation, proteasome, proteomics, ubiquitin carboxyl terminal hydrolase L-1.

J. Neurochem. (2004) **88**, 1540–1546.

The gracile axonal dystrophy (*gad*) mouse is an autosomal recessive spontaneous mutant that was identified in 1984 (Yamazaki *et al.* 1988). Pathologically, the *gad* mouse displays axonal degeneration of the gracile tract, which consists of thoracic, lumbar and sacral dorsal root ganglion axons. This axonal deterioration results in progressive sensory ataxia, and eventually spreads to the motor neurons and other centers in the CNS, causing paralysis and death after 150 days of age (Yamazaki *et al.* 1988). Accumulation of ubiquitin and amyloid-β protein deposits is also present along the sensory and motor nervous system (Wu *et al.* 1996).

Received October 14, 2003; revised manuscript received November 18, 2003; accepted November 20, 2003.

Address correspondence and reprint requests to Professor D. Allan Butterfield, Department of Chemistry and Center of Membrane Sciences, University of Kentucky, Lexington, KY 40506-0055, USA.
E-mail: dabcns@uky.edu

Abbreviations used: AD, Alzheimer's disease; DNP, dinitrophenyl hydrazone; DNPH, 2,4-dinitrophenylhydrazine; 2D PAGE, two-dimensional polyacrylamide gel electrophoresis; IPG, immobilized pH gradient; MS/MS, tandem mass spectrometry; UCH L-1, ubiquitin carboxyl-terminal hydrolase L-1.

The *gad* mutation has been identified as a deletion on chromosome 5 within the gene encoding ubiquitin carboxyl-terminal hydrolase L-1 (UCH-L1). The deletion lacks a segment of DNA corresponding to 42 amino acids containing the catalytic site of this protein (Saigoh *et al.* 1999). The role of UCH-L1 renders this mouse a suitable model for investigating neurodegenerative disorders, in which altered function of the ubiquitin system is present.

UCH L-1 is a crucial enzyme for maintaining protein degradation by the proteasome, by generating free monomeric ubiquitin (Osaka *et al.* 2003). Proteasomal dysfunction occurs in neurodegenerative disorders (Chung *et al.* 2001; Davies 2001; Ding and Keller 2001; Halliwell 2002). In Parkinson's disease there is genetic evidence for a contribution of UCH L-1 (Liu *et al.* 2002; Nishikawa *et al.* 2003; Jenner 2003). Our previous proteomic study (Castegna *et al.* 2002a) identified UCH L-1 as one specific target of protein oxidation in Alzheimer's disease (AD) brain, establishing a link between the effect of oxidative stress of brain proteins (Butterfield and Lauderback 2002; Butterfield *et al.* 2001; 2002) and the reported proteasomal dysfunction in AD. However, it is unclear how oxidation affects protein function, owing to the different responses of proteins to oxidation. Analysis of systems in which the oxidized protein displays lowered or null activity might represent an excellent model for investigating the effect of the protein of interest in cellular metabolism and evaluating how the cell responds to the stress caused by its oxidation.

Because of the lack of activity of UCHL-1 in *gad* mouse brain, this animal model was chosen to investigate the effect of dysfunctional UCH-L1 in brain in relation to specifically oxidized proteins. Proteomics appeared to be the most efficient way of performing this study because this method allows screening of both the expression and oxidation of hundreds of proteins at once.

Experimental procedures

Brain samples

Six wild-type and six *gad* mouse brain cortical samples (300 mg) were sonicated for 30 s in 500 µL two-dimensional polyacrylamide gel electrophoresis (2D PAGE) sample buffer (8 M urea, 2 M thiourea, 20 mM dithiothreitol, 0.2% (v/v) Biolytes 3–10, 2% CHAPS and bromophenol blue). Following centrifugation at 14000 *g* for 10 min, the supernatant was collected and the protein concentration was determined by using the RC DC assay (Bio-Rad, Hercules, CA, USA) as described previously (Castegna *et al.* 2002a,b, 2003).

2D PAGE and western blotting

2D PAGE was performed in a Bio-Rad system using 110-mm pH 3–10 immobilized pH gradient (IPG) strips and Criterion 8–16% gels (Bio-Rad). For the first dimension, 300 µg protein was applied to a rehydrated IPG strip, and isoelectric focusing was carried out at 20°C. Before the second-dimension separation, the gel strips were equilibrated for 10 min in 37.5 mM Tris-HCl (pH 8.8) containing 6 M urea, 2% (w/v) sodium dodecyl sulfate, 20% (v/v) glycerol and 0.5% dithiothreitol, and then re-equilibrated for 10 min in the same buffer except that dithiothreitol was replaced with 4.5% iodoacetamide. For detection of protein carbonyls, an index of protein oxidation (Butterfield and Stadtman 1997), Western blots (oxyblots) were obtained. The protein hydrazone was formed by incubating IPG strips with 10 mM 2,4-dinitrophenylhydrazine (DNPH)/1 M HCl for 10 min and 2 M Tris base/30% glycerol for 15 min. A detailed description of the chemistry involved in protein carbonyl formation and analysis has been published (Butterfield and Stadtman 1997). Basically, in the present study protein carbonyls were detected immunochemically by an antibody to the hydrazone formed between protein carbonyls and DNPH, followed by an alkaline phosphate-linked secondary antibody (Castegna *et al.* 2002a,b). The IPG strips were rehydrated as described above and placed on Criterion gels (Bio-Rad). After unstained molecular weight protein standards had been applied, electrophoresis was started. Isoelectric focusing was performed as follows: 300 V for 1 h, then linear gradient to 8000 V for 5 h and finally 20 000 V/h. Second-dimension gels were run at 200 V for 65 min (Butterfield and Castegna 2003). Immunoblotting analysis was performed as described in Castegna *et al.* (2002a).

Sample preparation for matrix-assisted laser desorption ionization-time of flight (MALDI-TOF) mass spectrometry

All mass spectra reported in this study were acquired by the University of Kentucky Mass Spectrometry Facility with an HP 1100 HPLC system modified with a custom splitter to deliver 4 µL/min to a custom C18 capillary column [300 µm (internal diameter) × 15 cm, packed in-house with Macrophere 300 5-µm C18 ; Alltech Associates, Deerfield, IL, USA]. Gradient separations consisted of 2 min isocratic at 95% water : 5% acetonitrile (both phases contain 0.1% formic acid) to begin with; the organic phase was increased to 20% acetonitrile over 8 min, then increased to 90% acetonitrile over 25 min, held at 90% acetonitrile for 8 min, then increased to 95% for 2 min, and finally returned to initial conditions for 10 min (total acquisition time 45 min with a 10-min recycle time). Tandem mass spectrometry (MS/MS) spectra were acquired on a Finnigan LCQ 'Classic' quadrupole ion trap mass spectrometer (Finnigan, Co., San Jose, CA, USA) in a data-dependent manner. Three scans were averaged to generate the data-dependent full scan spectrum. The most intense ion was subjected to tandem mass spectrometry, and five scans were averaged to produce the MS/MS spectrum. Masses subjected to the MS/MS scan were placed on an exclusion list for 2 min.

Tandem spectra used for protein identification from tryptic fragments were searched against the National Center for Biotechnology Information (NCBI) protein databases using a local MASCOT search engine server. Resulting MS/MS spectra assumed the peptides to be mono-isotopic, oxidized at methionine residues and carbamidomethylated at cysteine residues (Castegna *et al.* 2002a,b, 2003). However, a 0.8-Da MS/MS mass tolerance was used for searching. Only the MS/MS data provided identification of proteins, and a typical mass spectrum is represented in Fig. 1.

Probability-based MOWSE scores were estimated by comparison of search results against estimated random match population and were reported as $-10*\mathrm{LOG10}(p)$, where p is the absolute probab-

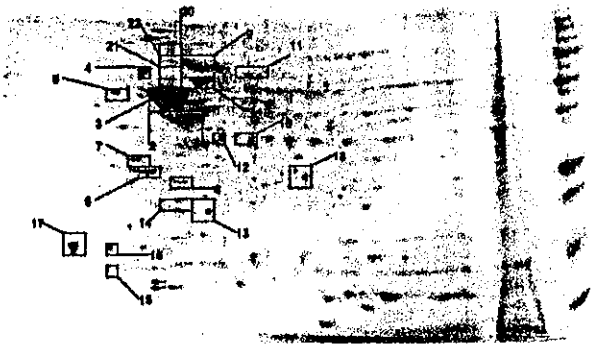

#	Protein
1	β-actin
2	Enolase
3	Tubulin
4	Neurofilament
5	Neurofilament
6	Tyrosine-3-monoxygenase
7	tyrosine 3/tryptophan 5 -monooxygenase activation protein
8	Rho GDP-dissociation inhibitor 1
9	Heat shock cognate 71 kDa protein
10	neurofilament protein NF-66
11	dihydropyrimidinase related protein-2
12	lactate dehydrogenase 2
13	RIKEN cDNA
14	thioredoxin peroxidase
15	hippocampal cholinergic neurostimulating peptide precursor
16	protein
17	β-synuclein
18	Calmodulin
19	phosphoglycerate mutase
20	malate dehydrogenase
21	Heat shock protein 86
22	dnaK-type molecular chaperone grp78 precursor or 78 kDa glucose-regulated protein precursor (GRP 78)
	Rab GDP dissociation inhibitor alpha & ATP synthase

Fig. 1 Example of liquid chromatography–MS/MS spectrum. In this case the spectrum is *m/z* 968 from gi/25742763 70-kDa heat-shock protein.

ility. All protein identifications were in the expected size range based on position in the gel.

Statistical analysis

Statistical comparison of carbonyl levels of proteins with anti-dinitrophenyl hydrazone (anti-DNP)-positive spots on 2D oxyblots from *gad* and wild-type, aged-matched control brain samples was by ANOVA. $p < 0.05$ was considered significantly different.

Results

DNPH-positive proteins on the blot were located in the gel map and excised for mass spectrometric analysis as described above. Twenty-two proteins were identified (Fig. 2). Proteins containing reactive carbonyl groups in *gad* and control brain samples were identified by 2D oxyblot analysis (Fig. 3). Comparison of 2D oxyblots with images of Coomassie blue-stained 2D gels from the same samples revealed that many, but not all, individual protein spots in the inferior parietal lobule brain extracts exhibit anti-protein carbonyl immunoreactivity. 2D oxyblots and the subsequent 2D gel images

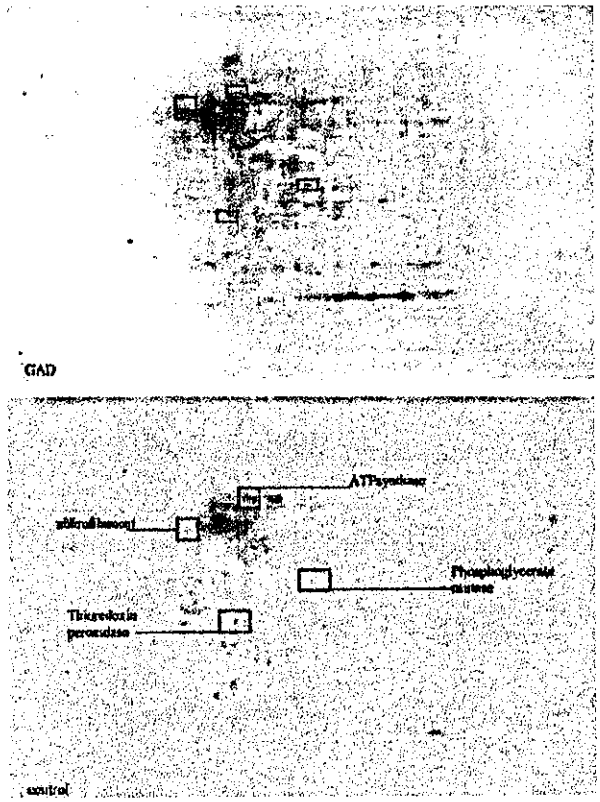

Fig. 2 D gel map of *gad* mouse brain. The proteins corresponding to the 22 spots identified by mass spectrometry are listed. As with most 2D gels, the pH increases from left to right on the abscissa, and molecular mass decreases from top to bottom on the ordinate.

were matched and the anti-DNP immunoreactivity of individual proteins separated by 2D PAGE was normalized to their protein content, obtained by measuring the intensity of colloidal Coomassie blue staining. This procedure allowed comparison of oxidation levels of brain proteins in *gad* and control subjects (Castegna *et al.* 2002a,b; Butterfield and Castegna 2003; Butterfield *et al.* 2003).

Only four proteins exhibited a significant increase in protein carbonyls in *gad* compared with control samples (Table 1). Three of these proteins were identified as phosphoglycerate mutase (1025 ± 187% of control), thioredoxin peroxidase (708 ± 123% of control) and neurofilament L (NF-L) (853 ± 13% of control). ATP synthase was identified together with Rab GDP dissociation inhibitor α; these two proteins have the same isoelectric point (pI) and molecular mass and it was impossible to separate them by 2D PAGE. The oxidation level for this mixture was 154 ± 43% of the wild-type spot. Table 2 presents the unique protein identifier (GI accession number), number of peptides identified, sequences determined, percentage sequence coverage, the probability-based MOWSE score and the *p* value for each oxidized protein identified. Note that the latter is exceedingly small, indicating that the identity established for each protein is correct.

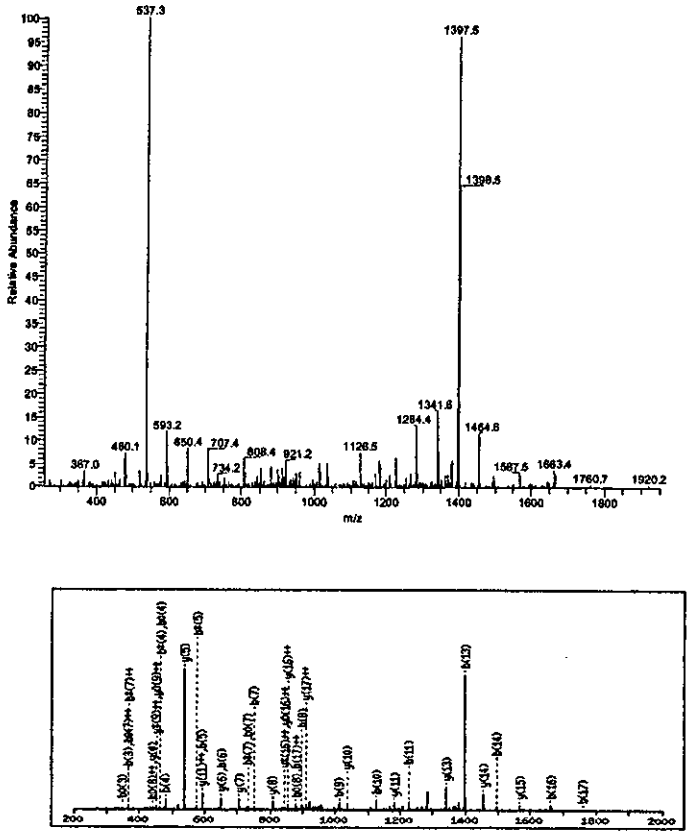

Fig. 3 Oxyblot maps for *gad* (top) and wild-type (bottom) mouse brain proteins, with labeled proteins significantly more oxidized in the *gad* mouse brain samples. The axes are the same as those in Fig. 1.

Discussion

The presence of non-functional UCH L1 in the *gad* mouse results in severe motor neuronal impairment. The results presented here give insight for the first time into the mechanism of neuronal degeneration in the *gad* mouse. Oxidative stress is responsible for NF-L disassembly, which in turn impairs axonal transport, causes demyelination and eventually leads to neuronal atrophy and death.

Table 1 Relative percentage change in specific carbonyl levels in proteomics-identified proteins in *gad* mouse brain compared with wild-type mouse control brain

Identified protein	Specific oxidation (% of control)	p^*
Phosphoglycerate mutase	1025 ± 187	0.05
Thioredoxin peroxidase	708 ± 123	< 0.05
Rab/ATPase (?)	154 ± 43	< 0.04
NF-L	853 ± 13	< 0.04

For each protein, individual anti-DNP immunostain/protein values (obtained from each of six *gad* and six control brains) were averaged and expressed as percentage of control ± SEM. *ANOVA.

Neurofilaments are axonal proteins that participate in the neuronal cytoskeletal structure and play an important role in the process of myelination. NF-L is a target of intensive study in motor neuron disease, in which abnormalities of its assembly, secondary structure and post-translational modifications have been detected (Crow *et al.* 1997; Beckman 1996; Chou *et al.* 1998; Cookson and Shaw 1999; Gelinas *et al.* 2000).

The abnormal accumulation of NF-L in degenerated motor neurons, which is the main pathological feature of amyotrophic lateral sclerosis (ALS), has initiated studies of the relationship between superoxide dismutase 1 mutation, which occurs in familial cases of ALS, and neurofilament accumulation. Superoxide dismutase-initiated nitration of mouse disassembled NF-L showed increases in 3-nitrotyrosine (Crow *et al.* 1997), consistent with the finding that tyrosine is often responsible for stabilization of neurofilament subunits, a stabilization fostered by hydrophobic interactions (Heins *et al.* 1993). Additionally, transgenic mice expressing a point mutation of NF-L exhibit motor impairment (Cote *et al.* 1993).

The hypothesis that neurofilaments might be a target of protein modification in motor neuron diseases in supported by extensive evidence (Beckman 1996; Chou *et al.* 1998; Cookson and Shaw 1999). Other than being targets of protein

Table 2 Proteomics characteristics of oxidatively modified proteins identified in *gad* mouse brain

Identified protein	GI accession no.	No. of peptides	Sequence	Sequence coverage (%)	MOWSE score	*p*
Phosphoglycerate mutase	gil8248819	5	LVLIR KAMEAVAAQGK + Oxidation(M) VLIAAHGNSLR NLKPIKPMQFLGDEETVR + Oxidation(M) HLEGLSEEAIMELNLPTGIPIVYELDK + Oxidation(M)	28	228	1.60×10^{-23}
Thioredoxin peroxidase (peroxiredoxin 2)	gil2499469	9	GVLR EYFSK SVDEALR GLFIIDAK NDEGIAYR SLSQNYGVLK SAPDFTATAVVDGAFK EGGLGPLNIPLLADVTK KEGGLGPLNIPLLADVTK	38	330	1.00×10^{-33}
Rab GDP dissociation inhibitor α	gil21903424	8	VVGVK LYSESLAR VVEGSFVYK FLMANGQLVK + Oxidation(M) KQNDVFGEADQ FQMLEGPPESMGR + 2Oxidation(M) NPYYGGESSSITPLEELYK YIAIASTTVETAEPEKEVEPALELLEPIDQK	23	388	1.60×10^{-39}
NF-L	gil20876600	20	DLR YVETPR LENELR FASFIER LLEGEETR KGADEAALAR ALYEQEIR YEEEVLSR LAAEDATNEK FTVLTESAAK AQLQDLNDR EYQDLLNVK VHELEQQNK MALDIEIAAYR + Oxidation(M) NMQNAEEWFK + Oxidation(M) IDSLMDEIAFLK + Oxidation(M) QNADISAMQDTINK + Oxidation(M) RIDSLMDEIAFLK + Oxidation(M) SAYSGLQSSSYLMSAR + Oxidation(M) SFPAYYTSHVQEEQTEVEETIEATK	35	864	3.90×10^{-67}

Oxidation (M); Oxidation of methionine.

nitration in ALS, neurofilament aggregates also bear advanced glycation endproducts in ALS conglomerates, indicating the susceptibility of neurofilament-L to oxidative insult.

The present finding of oxidized NF-L in *gad* mouse brain, a model for neuron motor disease, confirms previous data that provided evidence for the oxidation-related involvement of NF-L in motor neuron degeneration and established a common pattern for degeneration. If the results shown here for cortical tissue can be extended to spinal cord and motor neurons, the findings may be relevant to molecular mechanisms of neurodegeneration in ALS. Oxidation of NF-L implies modification of hydrophobic interactions that are responsible for the association of the different subunits. In fact, it has been demonstrated that the structure of neurofilament proteins is modified from α-helix to β-sheet

and random coil following free radical damage (Gelinas *et al.* 2000), directly relating oxidative damage of neurofilaments to the axonal degeneration in motor neurons. The consequences of neurofilament disassembly are deleterious to neuronal survival: the axonal antegrade and retrograde transport, which is essential for organelles, especially mitochondria which do not self-sufficiently synthesize most of the proteins necessary for their function, would be compromised.

Reduction of the fixed ubiquitin pool and decreased proteasomal function might lead to accumulation of oxidized proteins, which, in turn, might activate microglia and trigger an inflammatory response with production of free radicals. Such events, which might lead to neurodegeneration, might be exacerbated by the oxidation of thioredoxin peroxidase, which was also a target of oxidation in this *gad* mouse model of neurodegeneration. Thioredoxin peroxidases or peroxiredoxins are small redox proteins that act as antioxidants and catalyze the elimination of hydroperoxides through the reducing system thioredoxin/thioredoxin reductase. This enzyme is considered a strong defense against oxidative stress. Based on the loss of activity of other oxidatively modified brain proteins (Hensley *et al.* 1995; Butterfield *et al.* 1997), the finding of the present study that thioredoxin peroxidase is a target of protein oxidation in *gad* mouse brain implies harmful consequences for neurons in this UCH L-1-altered mouse, owing to a dramatic decrease in cellular antioxidant capability. Peroxiredoxin I/thioredoxin peroxidase 2 is up-regulated in ALS (Allen *et al.* 2003). Moreover, in oxidative stress induced by Fe^{2+} (Drake *et al.* 2002) or H_2O_2 (Mitsumoto *et al.* 2001) variant forms of peroxiredoxins have been identified. These investigations by others, coupled with the present finding that peroxiredoxin is oxidized in the *gad* mouse, are consistent with the existence of common downstream events in oxidative stress-induced neurodegeneration.

An oxidative stress-based mechanism of peroxiredoxin enzyme inactivation can be speculated: the enzyme bears two cysteine residues that are crucial for the antioxidant activity of thioredoxin peroxidase. Products of free radical-induced lipid peroxidation, such as 4-hydroxy-2-nonenal, can introduce carbonyls to proteins by covalent Michael addition to -SH groups of protein side chains (Butterfield and Stadtman 1997; Lauderback *et al.* 2001). Thus, it is conceivable that these cysteine proteins in peroxiredoxin are susceptible to attack by the excess 4-hydroxy-2-nonenal in neurodegenerative disorders associated with oxidative stress, including AD. Michael addition of 4-hydroxy-2-nonenal to brain proteins changes their structure and activity (Esterbauer *et al.* 1991; Subramaniam *et al.* 1997; Lauderback *et al.* 2001).

Phosphoglycerate mutase is the glycolytic enzyme responsible for the interconversion of 3-phosphoglycerate to 2-phosphoglycerate. Glycolytic enzymes and creatine kinase BB are oxidatively modified in AD brain (Castegna *et al.* 2002a, 2002b, 2003; Butterfield and Castegna 2003; Butterfield *et al.* 2003), and this oxidation might contribute to the reduced glucose metabolism observed in AD brain (Messier and Gagnon 1996), especially in the temporoparietal and frontal areas (Mielke *et al.* 1996). Although there is no evidence of involvement of energy metabolism depletion in the *gad* brain, the present finding that phosphoglycerate mutase was significantly more oxidized in *gad* brain than in control brain suggests a possible lower energy metabolism that might exacerbate the consequences of a lack of ATP necessary to carry out normal cellular function. Future studies should address this possibility.

Rab GDP dissociation inhibitor α and ATP synthase were detected as a single spot on the *gad* brain map, and the spot corresponding to these proteins showed increased carbonyl immunoreactivity. It is not possible at the present time to distinguish the extent of oxidation for the two proteins, the pI and molecular mass of which are practically identical. This result illustrates a limitation of 2D PAGE in separating proteins of similar size and charge distribution. Additional studies are required, perhaps using different isoelectric focusing strips with wider pH gradients, to separate the mixture into two detectable spots.

As seen in the present study, oxidative stress may be a source of protein damage by a vicious cycle, in which targets of oxidation may lead to further damage, as in the *gad* mouse. Further study of these connections is warranted. The present study demonstrates how the powerful tools of proteomics can provide insights into potential mechanisms of neurodegenerative disease. Continued use of proteomics analysis for the brain proteome in oxidative stress-related neurodegenerative disorders, and animal and culture models thereof, is in progress.

Acknowledgements

This work was supported in part by grants from the National Institutes of Health to DAB (AG-05119; AG-10836) and JK (R01 HL66358-01), and grants from the Ministry of Health, Labour and Welfare of Japan to KW and the Organization for Pharmaceutical Safety and Research of Japan to KW (MF-3).

References

Allen S., Heath P. R., Kirby J., Wharton S. B., Cookson M. R., Menzies F. M., Banks R. E. and Shaw P. J. (2003) Analysis of the cytosolic proteome in a cell culture model of familial amyotrophic lateral sclerosis reveals alterations to the proteasome, antioxidant defenses, and nitric oxide synthetic pathways. *J. Biol. Chem.* **278**, 6371–6383.

Beckman J. S. (1996) Oxidative damage and tyrosine nitration from peroxynitrite. *Chem. Res. Toxicol.* **9**, 836–844.

Butterfield D. A. and Lauderback C. M. (2002) Lipid peroxidation and protein oxidation in Alzheimer's disease brain: potential causes and consequences involving amyloid β-peptide-associated free radical oxidative stress. *Free Rad. Biol. Med.* **32**, 1050–1060.

Butterfield D. A. and Castegna A. (2003) Energy metabolism in Alzheimer's disease brain: insights from proteomics. *Appl. Genomics Proteomics* **2**, 67–70.

Butterfield D. A. and Stadtman E. R. (1997) Protein oxidation processes in aging brain. *Adv. Cell Aging Gerontol.* **2**, 161–191.

Butterfield D. A., Drake J., Pocernich C. and Castegna A. (2001) Evidence of oxidative damage in Alzheimer's disease brain: central role for amyloid beta-peptide. *Trends Mol. Med.* **7**, 548–554.

Butterfield D. A., Castegna A., Lauderback C. M. and Drake J. (2002) Review: evidence that amyloid beta-peptide-induced lipid peroxidation and its sequelae in Alzheimer's disease brain contributes to neuronal death. *Neurobiol. Aging* **23**, 655–664.

Butterfield D. A., Hensley K., Cole P., Subramanian R., Aksenova M., Aksenova M., Bummer P. M., Haley B. E. and Carney J. M. (1997) Oxidatively-induced structural alteration of glutamine synthetase assessed by analysis of spin label incorporation kinetics: Relevance to Alzheimer's disease. *J. Neurochem.* **68**, 2451–2457.

Butterfield D. A., Boyd-Kimball D. and Castegna A. (2003) Proteomics in Alzheimer's disease: insights into mechanisms of neurodegeneration. *J. Neurochem.* **86**, 1313–1327.

Castegna A., Aksenov M., Aksenova M., Thongboonkerd V., Klein J. B., Pierce W. M., Booze R., Markesbery W. M. and Butterfield D. A. (2002a) Proteomic identification of oxidatively modified proteins in Alzheimer's disease brain. Part I: creatine kinase BB, glutamine synthase, and ubiquitin carboxy-terminal hydrolase L-1. *Free Radic. Biol. Med.* **33**, 562–571.

Castegna A., Aksenov M., Aksenova M., Thongboonkerd V., Klein J. B., Pierce W. M., Booze R., Markesbery W. M. and Butterfield D. A. (2002b) Proteomic identification of oxidatively modified proteins in Alzheimer's disease brain. Part II: dihydropyrimidinase related protein II, α-enolase and heat shock cognate 71. *J. Neurochem.* **82**, 1524–1532.

Castegna A., Thongboonkerd V., Klein J. B., Lynn B., Markesbery W. M. and Butterfield D. A. (2003) Proteomic identification of nitrated proteins in Alzheimer's disease brain. *J. Neurochem.* **85**, 1394–1401.

Chou S. M., Wang H. S., Taniguchi A. and Bucala R. (1998) Advanced glycation endproducts in neurofilament conglomeration of motoneurons in familial and sporadic amyotrophic lateral sclerosis. *Mol. Med.* **4**, 324–332.

Chung K. K., Dawson V. L and Dawson T. M. (2001) The role of the ubiquitin–proteasomal pathway in Parkinson's disease and other neurodegenerative disorders. *Trends Neurosci.* **11**, S7–S14.

Cookson M. R. and Shaw P. J. (1999) Oxidative stress and motor neuron disease. *Brain Pathol.* **9**, 165–186.

Cote F., Collard J. F. and Julien J. P. (1993) Progressive neuronopathy in transgenic mice expressing the human neurofilament heavy gene: a mouse model of amyotrophic lateral sclerosis. *Cell* **73**, 35–46.

Crow J. P., Ye Y. Z., Strong M., Kirk M., Barnes S. and Beckman J. S. (1997) Superoxide dismutase catalyzes nitration of tyrosines by peroxynitrite in the rod and head domains of neurofilament-L. *J. Neurochem.* **69**, 1945–1953.

Davies J. J. (2001) Degradation of oxidized proteins by the 20S proteasome. *Biochimie* **83**, 301–310.

Ding Q. and Keller J. N. (2001) Proteasomes and proteasome inhibition in the central nervous system. *Free Radic. Biol. Med.* **31**, 574–584.

Drake S. K., Bourdon H., Wehr N. B., Levine R. L., Backlund P. S., Yergey A. L. and Rouault T. A. (2002) Numerous proteins in mammalian cells are prone to iron-dependent oxidation and proteasomal degradation. *Dev. Neurosci.* **24**, 114–124.

Esterbauer H., Schaur R. J. and Zollner H. (1991) Chemistry and biochemistry of 4-hydroxynonenal, malondialdehyde, and related aldehydes. *Free Radic. Biol. Med.* **11**, 81–128.

Gelinas S., Chapados C., Beauregard M., Gosselin I. and Martinoli M. G. (2000) Effect of oxidative stress on stability and structure of neurofilament proteins. *Biochem. Cell Biol.* **78**, 667–674.

Halliwell B. (2002) Hypothesis: proteasomal dysfunction: a primary event in neurodegeneration that leads to nitrative and oxidative stress and subsequent cell death. *Ann. N. Y. Acad. Sci.* **962**, 182–194.

Heins S., Wong P. C., Muller S., Goldie K., Cleveland D. W. and Aebi U. (1993) The rod domain of NF-L determines neurofilament architecture, whereas the end domains specify filament assembly and network formation. *J. Cell Biol.* **123**, 1517–1533.

Hensley K., Hall N., Sybramaniam R., Cole P., Harris M., Askenov M., Askenova M., Gabbita S. P., Wu J. F., Carney J. M., Lovell M., Markesbery W. R. and Butterfield D. A. (1995) Brain regional correspondence between Alzheimer's disease histopathology and biomarkers of protein oxidation. *J. Neurochem.* **65**, 2146–2156.

Jenner P. (2003) Oxidative stress in Parkinson's disease. *Ann. Neurol.* **53**, S26–S36.

Lauderback C. M., Hackett J. M., Huang F. F., Keller J. N., Szweda L. I., Markesbery W. R. and Butterfield D. A. (2001) The glial glutamate transporter, GLT-1, is oxidatively modified by 4-hydroxy-2-nonenal in the Alzheimer's disease brain: role of Aβ1–42. *J. Neurochem.* **78**, 413–416.

Liu Y., Fallon L., Lashuel H. A., Liu Z. and Lansbury P. T. Jr (2002) The *UCH L-1* gene encodes two opposing enzymatic activities that affect alpha-synuclein degradation and Parkinson's disease susceptibility. *Cell* **111**, 209–218.

Messier G. and Gagnon M. (1996) Glucose regulation and cognitive functions: relation to Alzheimer's disease and diabetes. *Behav. Brain Res.* **75**, 1–11.

Mielke R., Schroder R., Fink G. R., Kessler J., HerholZ. K. and Heiss W. D. (1996) Regional cerebral glucose metabolism and postmortem pathology in Alzheimer's disease. *Acta Neuropathol. (Berl.)* **91**, 174–179.

Mitsumoto A., Takanezawa Y., Okawa K., Iwamatsu A. and and Nakagawa Y. (2001) Variants of peroxiredoxins expression in response to hydroperoxide stress. *Free Radic. Biol. Med.* **30**, 625–635.

Nishikawa K., Li H., Kawamura R. *et al.* (2003) Alterations of structure and hydrolase activity of parkinsonism-associated human ubiquitin carboxyl-terminal hydrolase L1 variants. *Biochem. Biophys. Res. Commun.* **304**, 176–183.

Osaka H., Wang Y. L., Takada K. *et al.* (2003) Ubiquitin carboxy-terminal hydrolase L1 binds to and stabilizes monoubiquitin in neurons. *Hum. Mol. Genet.* **12**, 1945–1948.

Saigoh K., Wang Y. L., Suh J. G., Yamanishi T., Sakai Y., Kiyosawa H. *et al.* (1999) Intragenic deletion in the gene encoding ubiquitin carboxy-terminal hydrolase in *gad* mice. *Nat. Genet.* **23**, 47–51.

Subramaniam R., Roediger F., Jordan B., Mattson M. P., Keller J. N., Waeg G. and Butterfield D. A. (1997) The lipid peroxidation product 4-hydroxy-2-*trans*-nonenal alters the conformation of cortical synaptosomal membrane proteins. *J. Neurochem.* **69**, 1161–1169.

Wu J., Ichihara N., Chui D. H., Yamazaki K., Watabayashi T. and Kikuchi T. (1996) Abnormal ubiquitination of dystrophic axons in central nervous system of gracile axonal dystrophy (*gad*) mutant mouse. *Alzheimers Res.* **2**, 163–168.

Yamazaki K., Wasasugi N., Tomita T., Kicuchi T., Mukoyama M. and Ando K. (1988) Gracile Axonal Dystrophy (*gad*), a new neurological mutant in the mouse. *Proc. Soc. Exp. Biol. Med.* **187**, 209–215.

Heterogeneity and Potentiation of AMPA Type of Glutamate Receptors in Rat Cultured Microglia

YUKIKO HAGINO,[1] YUKIHIRO KARIURA,[1] YOSHIMASA MANAGO,[1] TAIJU AMANO,[1] BING WANG,[1] MASAYUKI SEKIGUCHI,[2] KAORI NISHIKAWA,[2] SHUNSUKE AOKI,[2] KEIJI WADA,[2] AND MAMI NODA[1]*

[1]*Laboratory of Pathophysiology, Graduate School of Pharmaceutical Sciences, Kyushu University, Fukuoka, Japan*

[2]*Department of Degenerative Neurological Diseases, National Institute of Neuroscience, National Center of Neurology and Psychiatry, Tokyo, Japan*

KEY WORDS whole-cell patch clamp; kainate; PEPA; cyclothiazide; flip; flop; RT-PCR; TNF-α

ABSTRACT α-amino-hydroxy-5-methyl-isoxazole-4-propionate (AMPA) receptor in rat cultured microglia were analyzed precisely using flop- and flip-preferring allosteric modulators of AMPA receptors, 4-[2-(phenylsulfonylamino)ethylthio]-2,6-difluoro-phenoxyacetamide (PEPA) and cyclothiazide (CTZ), respectively. Glutamate (Glu)- or kainite (KA)-induced currents were completely inhibited by a specific blocker of AMPA receptor, LY300164, indicating that functional Glu-receptors in cultured microglia are mostly AMPA receptor but not KA receptor in many cells. Glu- and KA-induced currents were potentiated by PEPA and CTZ in a concentration-dependent manner. The ratio of the potentiation by PEPA to the potentiation by cyclothiazide varied with cells between 0.1 and 0.9, suggesting cell-to-cell heterogeneity of AMPA receptor subunits expressed in microglia. Quantitative RT-PCR revealed that GluR1-3 mainly occurred in the flip forms, which agreed with the stronger potentiation of receptor currents by CTZ vs. PEPA. Finally, the potentiation of microglial AMPA receptors by PEPA and CTZ inhibited the Glu-induced release of tumor necrosis factor-α (TNF-α) unpredictably. The increase in TNF-α release by Glu or KA required extracellular Na^+ and Ca^{2+} ions but not mitogen-activated protein kinase (MAPK), suggesting the effects of PEPA and CTZ were not due to the inhibition of MAPK. These results suggest that potentiation of microglial AMPA receptors serves as a negative feedback mechanism for the regulation of TNF-α release and may contribute to the ameliorating effects of allosteric modulators of AMPA receptors.

INTRODUCTION

There is increasing evidence that functional glutamate (Glu) receptors are not restricted to neurons but also expressed in glial cells. Among glial cells, microglial cells express α-amino-hydroxy-5-methyl-isoxazole-4-propionate (AMPA)/kainite (KA) type of Glu receptors and the activation of Glu receptors triggered the release of tumor necrosis factor-α (TNF-α) from microglial cells (Noda et al., 2000). The neuron-glia interaction via Glu was proposed where microglia played an important role (Bezzi et al., 2001). Microglial cells are rapidly activated in response to even minor pathological changes so that they may be viewed as the cellular sensory element of brain pathology (Kreutzberg, 1996). Microglia likely contribute neurodegenerative diseases and dementia in AIDS (Streit

Grant sponsor: Grants-in-Aid for Scientific Research of Japan Society for Promotion of Science; Grant sponsor: Research Grant in Priority Area Research of the Ministry of Education, Culture, Sports, Science and Technology, Japan; Grant sponsor: Kyushu University Foundation; Grant sponsor: Grants-in-Aid for Scientific Research of the Ministry of Health, Labor and Welfare, Japan; Grant sponsor: the Organization for Pharmaceutical Safety and Research, Japan. Yukiko Hagino's present address is Daiichi Suntory Biomedical Research Limited, Osaka, Japan.

*Correspondence to: Mami Noda, Laboratory of Pathophysiology, Graduate School of Pharmaceutical Sciences, Kyushu University, Fukuoka 812-8582, Japan. E-mail: noda@phar.kyushu-u.ac.jp

Received 5 February 2003; Accepted 30 December 2003

DOI 10.1002/glia.20034

Published online 24 March 2004 in Wiley InterScience (www.interscience.wiley.com).

and Kincaid-Colton, 1995). Glu receptors in microglia may contribute to an important role especially in these pathological conditions. Therefore, detailed analyses on Glu receptor in microglia, for example, subunit composition and expression pattern, should be important for understanding the functional role of microglia.

Functional AMPA receptors are assembled tetramers (Sun et al., 2002) formed from subunits encoded by four different genes, GluR1, GluR2, GluR3, and GluR4 (Hollmann et al., 1989; Keinanen et al., 1990). Each subunit is known to exist as two isoforms, flip and flop, which are produced by alternative RNA splicing (Sommer et al., 1990). AMPA receptors consisting of different subunit and/or splice-variant combinations show different properties. For example, it has been found that incorporation of GluR2 into receptor complexes dramatically reduced calcium ion permeability of the receptor channel (Hollmann et al., 1991; Hume et al., 1991). Incorporation of differentially spliced isoforms into receptor complexes produces AMPA receptors with different desensitization profiles (Sommer et al., 1990; Mosbacher et al., 1994).

In the present study, we aimed to detect cell-to-cell heterogeneity of functional AMPA receptors in microglia by use of two allosteric potentiators of the receptors. One is 4-[2-(phenylsulfonylamino)ethylthio]-2,6-difluoro-phenoxyacetamide (PEPA), a flop-preferring modulator (Sekiguchi et al., 1997), and the other is cyclothiazide (CTZ), a flip-preferring modulator (Partin et al., 1994; Kessler et al., 2000). Both compounds suppress desensitization of AMPA receptors (Partin et al., 1996; Sekiguchi et al., 1997, 1998, 2002) and we already showed that cyclothiazide dramatically enhanced the AMPA receptor currents in microglia (Noda et al., 2000). Comparing the action of cyclothiazide with that of PEPA was an effective means for detecting flip/flop heterogeneity among AMPA receptors expressed in hippocampal neurons (Sekiguchi et al., 1998). Here, we show the heterogeneity of microglia based on the AMPA receptor expression.

In addition to the electrophysiological analyses, the effects of PEPA and cyclothiazide on the release of TNF-α from microglia were also investigated. We previously observed that Glu and KA stimulated TNF-α release from microglia (Noda et al., 2000). Surprisingly, potentiation of AMPA receptors by PEPA did not enhance TNF-α release from microglia but rather had opposite effects. These results suggest that the activation of AMPA receptors evoked complex signaling pathways to the TNF-α release event. Our data on the detection of heterogeneity and potentiation of AMPA receptors should be useful for further investigation on the functional role of microglia.

MATERIALS AND METHODS

Papain and DNase were purchased from Worthington Biochemical (Freehold, NJ). Eagle's medium (MEM) was obtained from Nissui (Tokyo, Japan). Fetal calf serum (FCS) was from Hyclone Laboratories (Logan, UT). KA, Glu, isolectin-B_4, and PD 098059 were purchased from Sigma Chemical (St. Louis, MO). CTZ and AMPA were from Tocris Cookson (Bristol, U.K.). PEPA was prepared as described previously (Sekiguchi et al., 1997, 1998) and LY300164 [7-acetyl-5-(4-aminophenyl)-8,9-dihydro-8-methyl-7H-1,3-dioxolo(4,5H)-2,3-benzodiazepine] was a gift from Eli Lilly (Surrey, U.K.).

Cell Culture

Microglial cells were isolated from the mixed cultures of cerebrocortical cells from postnatal day 3 Wistar rats (Kyudo, Kumamoto, Japan) as described previously (Noda et al., 1999). In brief, the cerebral cortex was minced and treated twice with papain (90 units) and DNase (2000 units) at 37°C for 15 min. The dissociated cells were seeded into 300 cm^2 plastic flasks at a density of 10^7 per 300 cm^2 in MEM or DMEM with 0.17% $NaHCO_3$ and 10% FCS and maintained at 37°C in 10% CO_2/90% air with a change of medium twice per week. After 10–14 days, floating cells and weakly attached cells on the mixed primary culture cell layer were obtained by gently shaking for 10–15 min. The resulting cell suspension was seeded onto glass coverslips and allowed to adhere for 30 min at 37°C. Then, microglia were isolated as strongly adhering cells after unattached cells were removed. The purity of microglia ranged from 95% to 99% according to the type of experiments. Special care was taken for PCR so that other cell types, for example, astrocytes and oligodendrocyte type 2 astrocyte (O-2A) progenitor cells, were not contaminated.

Cell Identification

Microglial cells were identified by a fluorescent probe, isolectin-B_4. Primary cultured microglia plated on the chamber slides were fixed with 4% paraformaldehyde for 30 min at room temperature, followed by a wash with phosphate-buffered saline (PBS). For the identification of microglia, the cells were treated with 10 μg/ml isolectin-B_4 overnight at 4°C, followed by 5 × wash with PBS. Then the cells were examined with a digital camera system (Axio Cam, Carl Zeiss, Germany) with high resolution mounted on a light and fluorescent microscope (Axioscope2 plus, Carl Zeiss).

Electrophysiological Measurements

Whole-cell recordings were made as reported previously (Noda et al., 1999, 2000) using an Axopatch-200B amplifier (Axon Instruments, Foster City, CA) under the voltage-clamp condition at the holding potential of −60 mV. The membrane currents were measured using a patch pipette containing (in mM): CsCl, 100; Na_2ATP, 3; N-2-hydroxyethylpiperazine-N′-2-ethan-